

Formation of Very Young Massive Clusters and implications for globular clusters

Sambaran Banerjee and Pavel Kroupa

To be published in *The Origin of Stellar Clusters*, ed. S. Stahler (Springer)

Abstract How Very Young Massive star Clusters (VYMCs; also known as “starburst” clusters), which typically are of $\gtrsim 10^4 M_\odot$ and are a few Myr old, form out of Giant Molecular Clouds is still largely an open question. Increasingly detailed observations of young star clusters and star-forming molecular clouds and computational studies provide clues about their formation scenarios and the underlying physical processes involved. This chapter is focused on reviewing the decade-long studies that attempt to computationally reproduce the well-observed nearby VYMCs, such as the Orion Nebula Cluster, R136 and NGC 3603 young cluster, thereby shedding light on birth conditions of massive star clusters, in general. On this regard, focus is given on direct N-body modeling of real-sized massive star clusters, with a monolithic structure and undergoing residual gas expulsion, which have consistently reproduced the observed characteristics of several VYMCs and also of young star clusters, in general. The connection of these relatively simplified model calculations with the structural richness of dense molecular clouds and the complexity of hydrodynamic calculations of star cluster formation is presented in detail. Furthermore, the connections of such VYMCs with globular clusters, which are nearly as old as our Universe, is discussed. The chapter is concluded by addressing long-term deeply gas-embedded (at least apparently) and substructured systems like W3 Main. While most of the results are quoted from existing and up-to-date literature, in an integrated fashion, several new insights and discussions are provided.

Sambaran Banerjee

AlfA/HISKP, University of Bonn, Auf dem Hügel 71, D-53121 Bonn, Germany, e-mail: sambaran@astro.uni-bonn.de

Pavel Kroupa

HISKP, University of Bonn, Auf dem Hügel 71, D-53121 Bonn, Germany, e-mail: pavel@astro.uni-bonn.de

1 Introduction

Very Young Massive Clusters (hereafter VYMCs) refer to a sub-category of star clusters which are $\gtrsim 10^4 M_\odot$ heavy (*i.e.*, massive) and a few Myr old in age, typically 1-3 Myr (*i.e.*, very young).¹ A number of such star clusters are observed in the molecular gas-dominated spiral arms (*e.g.*, the NGC 3603 Young Cluster) and in the central molecular zone (*e.g.*, the Arches and the Quintuplet clusters) of our Galaxy. They are also found in nearby disk galaxies of the local group (*e.g.*, the R136 cluster of the Large Magellanic Cloud) and in “starburst galaxies” (*e.g.*, in the Antennae Galaxies). An age $\lesssim 3$ Myr would imply that all of the massive stellar members of a VYMC are in their main sequences (MSs). The key importance of VYMCs is that being newly hatched, the details of their structure and internal kinematics can constrain the conditions under which massive star clusters, which are globular clusters at their infancy (Marks & Kroupa, 2012; Kruijssen, 2014), form. This allows one to distinguish between the different scenarios of massive cluster formation (Longmore et al., 2014). Note that the above mass and age limits defining VYMCs are meant to be generally true (see also Portegies Zwart et al. 2010) but not absolutely rigorous, to allow some well studied young systems, like the ONC ($\approx 10^3 M_\odot$), to be counted in as VYMCs.

Morphologically, VYMCs are often found as the richest core-halo member cluster of extended cluster complexes/stellar associations, *e.g.*, the ONC (Alves & Bouy, 2012). Young stellar systems are also found as extended associations of OB stars, *e.g.*, the Cygnus OB2 (Kuhn et al., 2014; Wright et al., 2014). It is also common to find them surrounded by HII (ionized hydrogen) gas (*e.g.*, NGC 3603 and R136; Pang et al. 2013). As for the sizes, the half-light radii of VYMCs are $\lesssim 1$ pc, *i.e.*, they are typically a factor of three more compact than Galactic globular clusters. This is consistent with VYMCs being infant globular clusters as their subsequent evolution due to mass segregation, dynamical encounters among stars and stellar binaries and stellar evolution would expand them. A handful of systems are found near-embedded in gas and highly compact; RCW 38 is a classic example where the HII-gas appears to have just begun releasing itself from the cluster (see below), exposing only the cluster’s central part (DeRose et al., 2009). Interestingly, several VYMCs are found to contain multiple density centers, *i.e.*, substructures, despite having an overall spherical core-halo morphology (Kuhn et al., 2014).

How (near) spherical parsec-scale VYMCs form out of vast, irregular molecular-hydrogen clouds is being widely debated for at least the past 10 years. Even without invoking any specific formation scenario, it can be said that dynamical relaxation (*i.e.*, statistical energy exchange among stars) must play a critical role in shaping the spherical core-halo structure of a VYMC. Hence, any formation channel for VYMCs must allow enough room for dynamical relaxation of the final (at an age of

¹ These objects are also popularly called “starburst” clusters. We prefer to call them Very Young Massive Clusters based on their characteristic properties, instead of referring to their likely starburst origin. The latter criterion may coincide with the origins of other types of massive clusters, *e.g.*, globular clusters. VYMCs constitute the youngest sub-category of Young Massive Clusters (YMCs; Portegies Zwart et al. 2010).

1-3 Myr) stellar assembly. The overall two-body relaxation time, that determines the secular (near dynamically stable) evolution, is typically several Gyr for a VYMC, which is much longer than its age. Hence, the present-day morphology of a VYMC is primarily dictated by what is called “violent relaxation” (Spitzer, 1987). The latter process refers to the energy redistribution among stars due to mutual encounters and rapid changes of the gravitational potential, leading to (near) dynamical equilibrium or “virialization” of the system, which happens in the timescale of stellar orbits (or in the dynamical timescale; Spitzer 1987; Heggie & Hut 2003), ² *i.e.*, typically in a fraction of a Myr. The observed *lack* of an age range among the members of the youngest star clusters (see, *e.g.*, Bastian & Silva-Villa 2013; Hollyhead et al. 2015) implies that these stars must have formed in a burst and integrated into a cluster over a short period of time.

Currently, there exist apparently at least two distinct scenarios for the formation of VYMCs. The “monolithic” or “episodic” or “in-situ” (top-down) scenario implies the formation of a compact star cluster in an essentially single but highly active star-formation episode (a “starburst”). The infant cluster of pre-main-sequence (PMS) and main sequence (MS) stars remains embedded in its parent molecular gas cloud. The latter eventually gets ionized by the UV radiation from the massive stars and receives energy from stellar mass outflows and due to coupling with stellar radiation. Such energy injection eventually causes the embedding gas to become gravitationally unbound from the system and to disperse in a timescale typically comparable to the dynamical time of the stellar system, *i.e.*, too fast for the stars to adjust with the corresponding depletion of the potential well. This causes the stellar system to expand violently and lose a fraction of its stars depending on its initial mass and concentration (Lada et al., 1984; Adams, 2000; Boily & Kroupa, 2003a,b; Baumgardt & Kroupa, 2007). The remaining system may eventually regain virial or dynamical equilibrium (re-virialization); hence a given VYMC may or may not be in equilibrium depending on the time taken to re-virialize and the epoch of its observation (Banerjee & Kroupa, 2013). Such a monolithic or top-down cluster formation scenario has successfully explained the details of well observed VYMCs, *e.g.*, ONC (also the Pleiades; Kroupa et al. 2001), R136 (Banerjee & Kroupa, 2013) and the NGC 3603 young cluster (Banerjee & Kroupa, 2014).

Alternatively, VYMCs are thought to have formed “bottom-up” through hierarchical merging of less massive subclusters (Longmore et al., 2014). Several of such subclusters fall onto each other and coalesce to form the final VYMC. The gravitational potential of the background molecular gas within which these subclusters appear makes the infall faster (the so-called “conveyor belt mechanism”; Longmore et al. 2014). The observational motivation for such a scenario is the apparent substructures in OB associations and even in VYMCs with overall core-halo configurations (Kuhn et al., 2014).

As of now, star formation has been studied in hydrodynamic calculations involving development of seed turbulences, in cubical/spherical gas clouds, into high-

² This timescale is commonly represented by the orbital “crossing time” which is the time taken to traverse the spatial scale of the system (say, its half mass diameter) by a particle moving radially with the dispersion speed.

density filaments where star formation occurs as a result of gravitational collapse and fragmentation (Klessen et al., 1998; Bate & Bonnell, 2004; Girichidis et al., 2011). In all such smoothed-particle-hydrodynamic (SPH) calculations, a hydrodynamic “sink particle”³ is physically associated with a proto-star. In these computations, clusters of proto-stars are formed within high-density filaments and/or filament junctions, which then fall collectively into the gravitational potential well of the cloud to form larger (gas-embedded) clusters (*e.g.*, in Bate 2009 and Girichidis et al. 2011). Different groups have reached the state-of-the-art of such calculations by including different details of the relevant physical processes but for mass scales much lighter than VYMCs. Such SPH calculations, requiring very high particle resolution, is prohibitive for the mass range of VYMCs ($> 10^4 M_\odot$).

High-resolution (reaching the “opacity limit”) SPH computations have so far been done forming stars in spherical gas clouds of up to $\approx 500 M_\odot$ only (Klessen et al., 1998; Bate & Bonnell, 2004; Bate, 2009; Girichidis et al., 2011, 2012; Bate, 2012) but without any feedback and hence self-regulation mechanism, which is critical in determining the star formation efficiency (SFE). Radiation-magnetohydrodynamic (MHD) calculations including stellar feedback (radiation and matter outflows) to the star-forming gas have also been carried out from proto-stellar scales (Machida & Matsumoto, 2012; Bate et al., 2014) up to $\approx 50 M_\odot$ gas spheres (Price & Bate, 2010). While the latter studies provide insights into the self-regulation mechanisms in the star formation process and point to an SFE near 30%, the scenario of the ultimate dispersal of the residual gas still remains superficial. See Krumholz et al. (2014) for an up-to-date review. Note, however, that the gas must disperse from the region in the molecular cloud where the cluster ultimately assembles, to obtain a gas-free young cluster like what we see today.

Therefore, as it turns out, the majority of the published studies to date related to the formation and evolution of “real-sized” VYMCs treat the gas-dispersal phase by including a time-varying external analytical potential (see Sec. 2.2) mimicking the residual gas (*e.g.*, Adams 2000; Kroupa et al. 2001; Baumgardt & Kroupa 2007; Pfalzner & Kaczmarek 2013; Banerjee & Kroupa 2013, 2014). This captures the essential dynamical effects of the gas dispersal. The dynamical evolution of the cluster, however, is treated accurately using direct N-body integration (Aarseth, 2003), in most of such works. This approach has successfully explained several well observed VYMCs, *e.g.*, the Galactic ONC (Kroupa et al., 2001) and NGC 3603 young cluster (Banerjee & Kroupa, 2014) and R136 (Banerjee & Kroupa, 2013) of the LMC. Such studies point to a universal SFE of $\epsilon \approx 33\%$ and a near-sonic dispersal of the residual HII gas (see Banerjee & Kroupa 2013 and references therein), remarkably reproducing the measured kinematic and structural properties of these clusters.

On the other hand, the dynamical process of coalescence of subclusters into more massive clusters has also been studied recently using direct N-body calculations in both absence (*e.g.*, Fujii et al. 2012) and presence (*e.g.*, Smith et al. 2013) of a

³ A “sink particle” is a dense, self-gravitating region in a fluid field approximated by a point mass for facilitating calculations (Klessen et al., 1998). A sink particle can only grow in mass by accreting matter from its surrounding.

background gas potential. The role of this process is also investigated in the context of formation of dwarf galaxies through merger of young massive clusters (Kroupa, 1998; Fellhauer & Kroupa, 2005; Amaro-Seoane et al., 2014).

The goal of the present chapter is to comprehend the most recent studies on the formation of VYMCs. Although most of these works treat the star forming gas indirectly as mentioned above, they incorporate the mass and spatial scales appropriate for VYMCs and capture the essential physics at the same time. Extrapolation of the results from hydrodynamical calculations over a large mass range, *i.e.*, from the computationally accessible masses (see above) to the realistic values, is unreliable since the scalings of all the relevant physical processes are not known and also they scale differently. This leaves us with the analytical treatment of the residual gas (Sec. 2.2) as the only viable option to directly treat VYMC-scale systems, given the present state of technology.

In Sec. 2 of this chapter, we discuss the monolithic formation scenario in greater detail. We focus on those (theoretical) studies that have addressed well observed VYMCs. The central young cluster HD 97950 (hereafter HD97950) of the Galactic NGC 3603 star-forming region is always of particular interest in this regard since, due to its proximity, it is perhaps the best observed VYMC. Next, in Sec. 3, we move on to discuss further on the hierarchical formation of VYMCs. Here, we again focus on HD97950 cluster whose structure is known in detail. This enables us to directly compare the two formation channels and put constraints on the initial conditions in each case. In Sec. 5, we conclude this chapter by discussing how VYMCs can be related to embedded clusters.

Technology, at present, does not permit self-consistent hydrodynamic calculations of star cluster formation, with adequate resolution and including feedback at the same time, for masses relevant for young massive clusters ($\gtrsim 10^4 M_\odot$). While such hydrodynamic calculations are doable with gas clouds of much lower masses (up to $100 M_\odot$ s), a large extrapolation is grossly unreliable since the physical processes involved are not all well understood (*e.g.*, gravitational fragmentation, role of magnetic field) and they scale differently. An analytic treatment of the gas combined with N-body calculation of the star cluster is, at present, the only viable way to reach such mass scales.

2 Monolithic or episodic formation of Very Young Massive Clusters

Before going into any details of modelling, one can obtain preliminary estimates that signifies the role of violent relaxation in the formation of VYMCs. For a self-bound system in dynamical (or virial) equilibrium with total K.E., T , and total P.E., V , the virial condition is satisfied (Spitzer, 1987), *i.e.*,

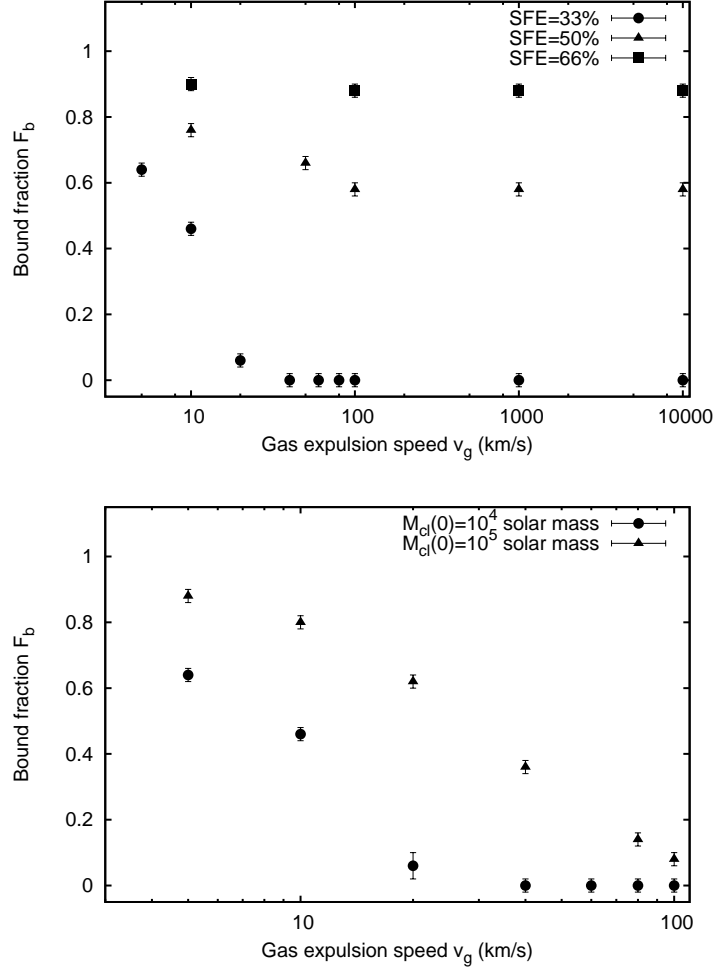


Fig. 1 Bound fraction, F_b , of a star cluster as a function of the overall gas removal speed, v_g , with varying star formation efficiency, ϵ ($M_{cl}(0) = 10^4 M_\odot$, $r_h(0) = 0.3$ pc; top panel), and initial stellar cluster mass, $M_{cl}(0)$ ($\epsilon = 0.33$, $r_h(0) = 0.3$ pc; bottom panel). All the initial clusters follow a Plummer density distribution. These results are obtained from NBODY6 computations. See text for details. The authors thank Nina Brinkmann of the AIfA, Bonn for providing aid in preparing this figure.

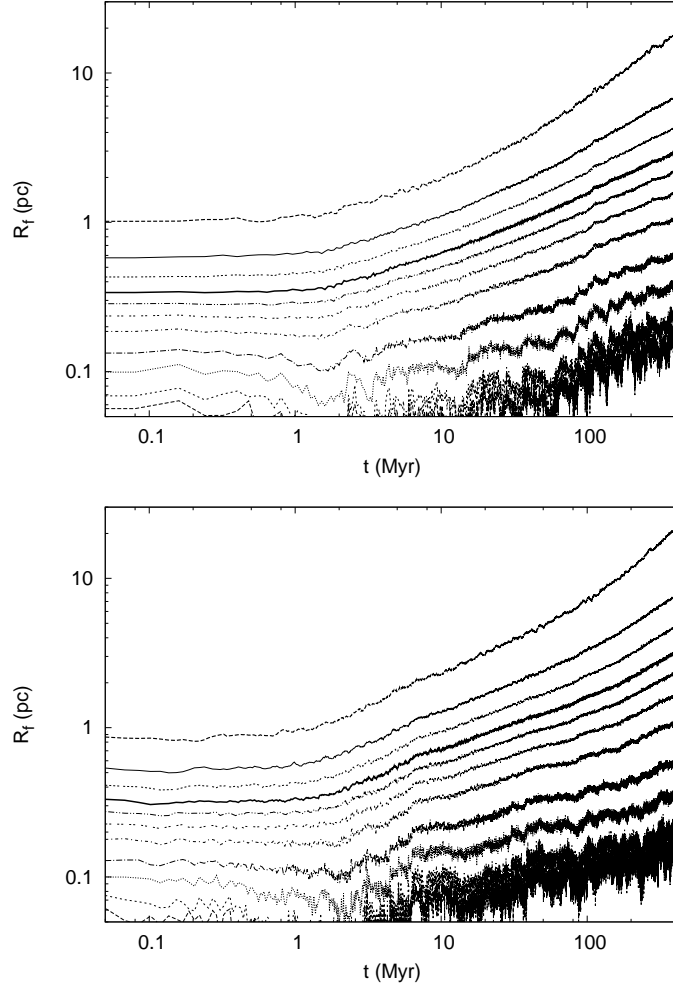


Fig. 2 Evolution of the overall size of an initial Plummer star cluster, with initial mass $M_{cl}(0) \approx 1.3 \times 10^4 M_{\odot}$ and half mass radius $r_h(0) \approx 0.3$ pc, as shown by the Lagrange radii. These clusters are taken to be isolated. The upper and the lower panels are obtained from NBODY6 calculations without and with primordial binaries (Kroupa 1995b; see text) respectively. These computed clusters are *not* subjected to any residual gas expulsion and their evolution is solely due to dynamical processes (two-body relaxation, close encounters and ejections) and stellar evolution. These lead to an overall slow expansion of the cluster due to dynamical heating and mass loss. In both panels, the curves are the Lagrange radii R_f of mass fraction f where $f = 0.01, 0.02, 0.05, 0.1, 0.2, 0.3, 0.4, 0.5, 0.625, 0.7$ and 0.9 from bottom to top respectively. The thick solid line is therefore the half mass radius, $r_h(t)$, of the cluster. The secular evolution hardly expands the initially compact cluster within 3 Myr age and it takes several 100 Myr to expand it by several factors (in terms of r_h), both in absence or presence of a realistic population of primordial binaries.

$$2T = -V. \quad (1)$$

For an “explosive” gas expulsion (see Sec. 1; Kroupa 2005), *i.e.*, gas removal in a timescale, τ_g , smaller or comparable to the crossing time, τ_{cr} , of the system (see below), T remains nearly unchanged right after the gas is removed although the P.E. drops to V' . The scale length of the system, r_h , usually taken as its half mass radius, also remains nearly unchanged.

For the overall system to remain bound after the gas expulsion, one must have,

$$T + V' \leq 0. \quad (2)$$

If M and M' are the total systemic masses before and just after the mass depletion respectively, then $V = -GM^2/r_h$ and $V' = -GM'^2/r_h$. Hence, using Eqn. 1,

$$M'^2 \geq \frac{M^2}{2}, \quad (3)$$

or

$$M' \gtrsim 0.7M. \quad (4)$$

For the present case, $M = M_{tot}$ is the total mass of the residual gas and the stars in the cluster, before the gas expulsion, and $M' = M_*$ is the total stellar mass after the depletion. Hence,

$$M_* \gtrsim 0.7M_{tot}. \quad (5)$$

In other words, for the cluster to survive the gas expulsion, its SFE should be $\varepsilon = M_*/M_{tot} \gtrsim 70\%$. This requirement is in contrast with realistic values of SFE which is $\varepsilon \lesssim 30\%$ as supported by both observations (Lada & Lada, 2003) and theoretical studies (Machida & Matsumoto 2012; Bate et al. 2014; see below). This alone would invalidate the monolithic cluster formation scenario since all clusters would dissolve even for the maximum SFE.

In practice, however, violent relaxation⁴ among the stars in the expanding cluster generates a “fallback effect” which retains a fraction of gravitationally-bound stars even for SFE $\lesssim 30\%$ (also see Boily & Kroupa 2002). The resultant bound fraction, F_b , depends on how efficiently stars in the expanding post-gas-expulsion cluster exchange energy during this relaxation process. Hence, F_b is proportional to the central stellar concentration (total stellar mass vs. size) of the pre-gas-expulsion cluster and to the timescale of the gas expulsion (time over which the expanding system remains in a dense enough phase for efficient energy exchange). In other words, F_b is proportional to the efficiency of violent relaxation which ultimately scales with the stellar number density. The latter is governed by the stellar density

⁴ In a self-gravitating system which is in dynamical equilibrium, the orbital energy exchange among stars by two-body encounters occur differentially among similar orbits (apart from that in occasional close encounters). This “two-body relaxation” drives the overall quasi-static secular evolution of the system which happens on the timescale of many orbital crossing times. However, if the system is not in equilibrium, the energy exchange happens much faster, in crossing times. Such “violent relaxation” drives the system (or a fraction of it) towards dynamical equilibrium (or energy minimum). See, *e.g.*, Spitzer (1987) for details.

of the pre-gas-expulsion cluster. Note that for a given (fractional) rate of gas removal and a pre-gas-expulsion stellar density, the resulting efficiency of violent relaxation limits the expansion of the initial (bound) stellar system and the time in which the bound fraction returns to equilibrium (or the re-virialization time; see Sec. 2.3.2).

Fig. 1 shows the bound fraction as a function of the initial (pre-gas-expulsion) cluster stellar mass, $M_{cl}(0)$, and the effective speed, v_g , at which the gas is expelled. v_g directly translates into the gas expulsion timescale (e-folding time; see below), τ_g , since $\tau_g = r_h(0)/v_g$. The observed trend in Fig. 1 is what is expected from the above discussion.

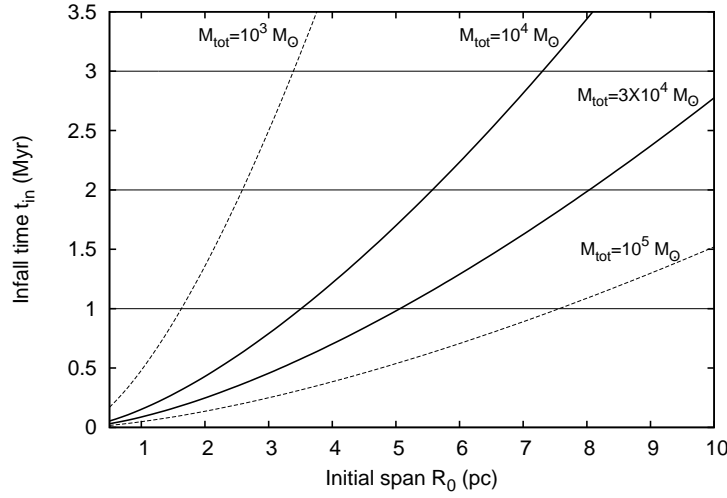


Fig. 3 The infall time (or the time of first arrival at orbital pericenter) of the subclusters, t_{in} , as a function of the radius, R_0 , of the spherical volume over which they are initially distributed. The curves are according to Eqn. 6 for different systemic mass M_{tot} . The highlighted curves for $M_{tot} = M_* = 10^4 M_\odot$ without a residual gas and $M_{tot} = 3M_* = 3 \times 10^4 M_\odot$ correspond to the model calculations for the NGC 3603 young cluster (see Sec. 3). This figure is reproduced from Banerjee & Kroupa (2015).

2.1 Why is an episodic or monolithic mode of cluster formation necessary?

The conditions in star forming molecular clouds in our Galaxy, which can be considered representative of star forming environments in gas-rich galaxies, do not necessarily imply cluster formation in a single go (see Sec. 1). Such molecular regions typically contain compact, interconnected filamentary structures as revealed by detailed observations, *e.g.*, by the *Herschel* space telescope. These observations

(André et al., 2014) reveal clusters of proto-stars forming within such high-density filaments (or ridges), which are found to have Plummer-like cross sections with radii of 0.1-0.3 pc, and at their junctions, implying a highly substructured initial condition for newborn stellar associations. This is also consistent with several observed stellar associations that contain individual stellar groups (*e.g.*, the Taurus-Auriga or T-A association; Palla & Stahler 2002) or are highly substructured (*e.g.*, Cygnus OB2; Wright et al. 2014), indicating an amorphous and substructured beginning of a star cluster as is often argued (see, *e.g.*, Longmore et al. 2014). On the other hand, VYMCs are found with near spherical core-halo profiles at a few Myr age which does not add up with the above scenario and calls for a different, episodic regime of cluster formation.

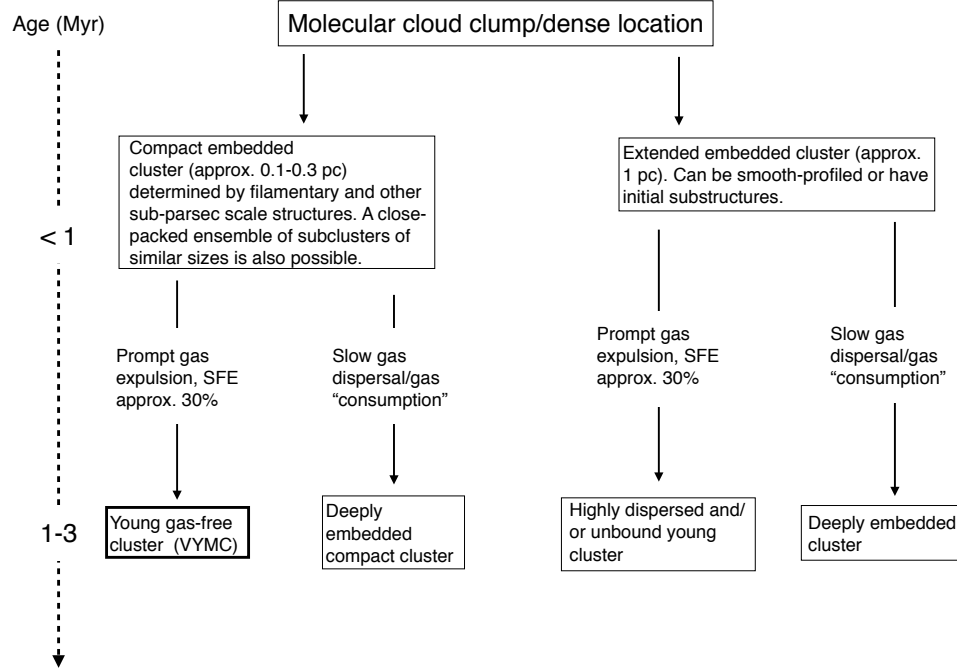


Fig. 4 Flowchart showing that exposed young massive clusters of 1-3 Myr age can form through essentially only one channel; a highly compact gas embedded proto-cluster undergoing a substantial ($\approx 70\%$ by mass) and rapid (in a timescale comparable to the crossing time of the proto-cluster) gas removal.

Of course, a stellar assembly cannot appear with 100% SFE since star formation is quenched by stellar radiative and mechanical feedback. Hydrodynamic simula-

tions (*e.g.*, Machida & Matsumoto 2012; Bate et al. 2014) including stellar feedback and observations of embedded stellar assemblies in the solar neighborhood (Lada & Lada, 2003) both indicate SFE $\lesssim 30\%$. Hence a substantial gas dispersal should accompany such a monolithic cluster formation to expose the gas-free young cluster. Arguably, several VYMCs, despite their near spherical monolithic structure contain substructures in the form of multiple density maxima in their surface stellar density profiles (Kuhn et al., 2014). Here, such systems will also be called monolithic.

The present day sizes of gas-free massive, young clusters, with half mass radii, r_h , between 3 - 10 pc is itself indicative of the importance of gas expulsion in the formation of such systems (Pfalzner, 2009). Observations suggest that newborn (*i.e.*, embedded) clusters are highly compact — typically with half mass radii $r_h < 1$ pc (see below). It is nearly impossible to expand such compact clusters up to their present day sizes through purely secular evolution. Fig. 2 shows the evolution of the Lagrange radii of a cluster with $M_{cl}(0) \approx 1.3 \times 10^4 M_\odot$ and $r_h(0) \approx 0.3$ pc as obtained through direct N-body calculation using the state-of-the-art NBODY6⁵ code. Here, the cluster expands only by a factor of few in ≈ 100 Myr, due to dynamical interactions and mass loss due to stellar evolution; it hardly expands in a few Myr age. Hence, an additional expansion mechanism is essential to explain the observed cluster sizes. As explained below, the above initial $r_h(0) \approx 0.3$ pc is the most plausible one as supported by observational and theoretical studies of birth conditions of star clusters.

The strongest support for an episodic mode of star formation is what can be called the “timescale problem” of cluster assembly. Consider a system of stellar clumps (or subclusters) of total mass M_* within a spherical volume of radius R_0 , which have zero or small relative speeds (see Sec. 3). In other words, they form a “cold” system which can fall in and assemble into a single bound star cluster. An embedding background molecular gas of total mass M_g would accelerate the infall; the so called “conveyor belt” mechanism (Longmore et al., 2014). The time, t_{in} , for the subclusters to collide onto each other at the systemic potential minimum is given by (Banerjee & Kroupa, 2015)

$$t_{in} \approx \frac{R_0^{\frac{3}{2}}}{\sqrt{GM_{tot}}} = 0.152 \frac{\left(\frac{R_0}{\text{pc}}\right)^{\frac{3}{2}}}{\left(\frac{M_{tot}}{10^4 M_\odot}\right)^{\frac{1}{2}}} \text{ Myr}, \quad (6)$$

where $M_{tot} = M_* + M_g$. Fig. 3 shows the dependence of t_{in} on typical masses and sizes involved in massive stellar associations.

⁵ Sverre Aarseth’s code NBODY6 and its variants (Aarseth, 2012) are presently the most advanced and realistic direct N-body evolution code. The N-body integration engine computes individual trajectories of all the stars using a fourth-order Hermite scheme. Close encounters are dealt with two- and multi-body regularizations. In addition, the code employs the BSE stellar and binary evolution scheme (Hurley et al., 2000) for evolving the individual stars and mass-transferring binaries. The code also includes recipes for tidal interactions and stellar collisions. See Aarseth (2003) for details.

Note that the above t_{in} estimates the time taken for the subclusters to meet each other *for the first time*, after which they pass through each other to continue in their orbits. The orbital energy of the subclusters is dissipated into the orbital energy of the individual stars during their each mutual passage due to violent relaxation, causing the subclusters' orbits to decay and finally merge into a single cluster in dynamical equilibrium. Hence, the final merger time, t_{mrg} , is several t_{in} s as found in N-body calculations (Sec. 3). Although t_{in} decreases with increasing background gas mass, M_g , this does not necessarily lead to shorter t_{mrg} as the subclusters approach faster and hence take larger number of orbits to dissipate their K.E. As found in N-body calculations, the background gas actually lengthens t_{mrg} (see Sec. 3 for the details) for $R_0 \gtrsim 2$ pc. In other words, the conveyor belt process does not necessarily accelerate the assembly of the final cluster. Hence, Fig. 3 implies that unless a group of subclusters form too close to each other, *i.e.*, already within the length scale of a compact star cluster (a few pc), it is practically impossible to assemble a VYMC by its young age through sequential mergers of less massive substructures as found in star-forming molecular clouds; see Sec. 3 for more details. Therefore, it is far more likely that VYMCs form in cluster- or molecular clump-scale localized high efficiency star formation episodes, *i.e.*, monolithically.

Interestingly, based on the observed velocity fields of gas clouds in the neighborhood of several starburst clusters, some authors (Furukawa et al., 2009; Fukui et al., 2014, 2015) suggest that these clusters (*e.g.*, Westerlund 2, NGC 3603) form out of intense starbursts triggered during major cloud-cloud collisions. Such conclusions are based on the observed “broad-bridge” features (Haworth et al., 2015) in the velocity-space morphologies of cloud fragments near these VYMCs. A collision between a pair of massive molecular clouds lasts for a short time, typically ≈ 1 Myr. Hence, as before, this points to an episodic formation of these VYMCs during the cloud-cloud collisions. After the clouds have crossed each other, the depletion of the background potential would lead to an expansion of the newly-hatched cluster, as in the case of internal gas expulsion. However, more detailed studies of the internal velocities of such gas clouds and as well further theoretical studies of cloud-cloud collisions (Duarte-Cabral et al., 2011; Takahira et al., 2014) is necessary to establish this scenario.

Finally, one can ask the following question: *What if a VYMC is simply formed in-situ but with its current observed size and not being governed by compact molecular filaments or other compact structures of the molecular clouds, eliminating the need of a substantial rapid gas dispersal?* In that case, the cluster must form with a sufficiently high SFE. However, it is unlikely that SFE can be pushed beyond $\approx 30\%$ as observational and theoretical studies suggest (see Sec. 2.2.1). Hence, such a scenario is unrealistic. With SFE near 30%, a typical present-day sized star cluster would largely become unbound and/or become too extended, depending on its initial mass. The cluster can, however, survive if the gas is dispersed slowly; in a timescale longer than a few crossing times (Lada et al., 1984). The ambient gas can also be depleted if it is accreted by the (proto-) stars (“gas consumption”; Longmore et al. 2014), without expanding or unbinding the cluster. These processes would, however, take much longer than a few Myr and one would obtain an embedded cluster instead, like

W3 Main. Further discussions follow in Sec. 5. The flowchart in Fig. 4 summarizes the discussions in this section.

The typical present-day density ($10^4 - 10^5 M_\odot \text{ pc}^{-3}$; or size $\approx 1 \text{ pc}$), age ($\approx 1 - 3 \text{ Myr}$) and (near) spherical core-halo morphology of gas-free very young massive clusters (VYMCs), like R136, NGC 3603 and the ONC, dictate an episodic or monolithic (or near monolithic) formation of such star clusters, undergoing a violent gas dispersal phase.

2.2 An analytic representation for gas expulsion

The episodic cluster formation scenario involving gas expulsion, which is widely used (Lada et al., 1984; Adams, 2000; Kroupa et al., 2001; Boily & Kroupa, 2002; Baumgardt & Kroupa, 2007; Banerjee & Kroupa, 2013, 2014; Pfalzner & Kaczmarek, 2013), has been successful in explaining the detailed structure and several well observed VYMCs. All these studies use a rather straightforward initial condition of a Plummer star cluster of mass, $M_{cl}(0)$,⁶ and half mass radius, $r_h(0)$, that is embedded in its spherically symmetric natal gas of total mass $M_g(0)$. The latter is assumed to have a constant SFE, ϵ , throughout, *i.e.*, the gas density profile follows the stellar Plummer density profile. The initial system represents a dense molecular gas clump with a recent episode of star formation with efficiency ϵ . The initial mass function (IMF) of the stellar system can be plausibly represented by the canonical mass function (Kroupa, 2001; Kroupa et al., 2013) although equal mass stars have also been used in the literature for scalability (*e.g.*, Baumgardt & Kroupa 2007; Pfalzner & Kaczmarek 2013).

As discussed above, the gas component is treated simply as an analytical external (Plummer) potential corresponding to its mass distribution whereas the stellar system is tracked accurately using direct N-body calculations, which captures the essential dynamics of the stellar system. The escape of the gas component is typically modelled as an exponential decay of the gas mass with e-folding time τ_g after a “delay time” τ_d , *i.e.*,

$$\begin{aligned} M_g(t) &= M_g(0) & t \leq \tau_d, \\ M_g(t) &= M_g(0) \exp\left(-\frac{(t-\tau_d)}{\tau_g}\right) & t > \tau_d. \end{aligned} \quad (7)$$

τ_g is determined by the effective speed, v_g , with which the gas escapes out, *i.e.*, $\tau_g \approx r_h(0)/v_g$. The Plummer radius of the gas distribution is kept fixed at $r_h(0)$. Such an analytic treatment of the gaseous component is justified by Geyer & Burkert (2001) who show that expelling the gas analogously by detailed SPH calculations (using shock heating) and analytically produce similar effect on the stellar system.

⁶ For monolithic systems we denote here the stellar mass as $M_{cl} \equiv M_*$.

Note that the corresponding (clump) SFE is $\varepsilon = M_{cl}(0)/(M_{cl}(0) + M_g(0))$ or

$$M_g(0) = M_{cl}(0) \left(\frac{1}{\varepsilon} - 1 \right) \quad (8)$$

2.2.1 Parameters for gas expulsion

One key parameter in the above model of the initial phase of cluster formation is the initial size of the embedded system given by its half mass radius $r_h(0)$. While in the literature there is no norm in the choice of the compactness of the gas-filled system, detailed observations of molecular clouds and embedded proto-stars imply highly compact profiles of proto-stellar clusters. As seen in the *Herschel* observations, and more recently using the *ALMA*, proto-stellar associations appear in the highly compact filamentary overdensities and in their junctions (Schneider et al., 2010, 2012; Hill et al., 2011; Hennemann et al., 2012; Tafalla & Hacar, 2015) in giant molecular gas clouds (GMCs). The sections of these filaments are very compact; typically $\lesssim 0.3$ pc and peaked at ≈ 0.1 pc (André et al., 2011). The profiles of these filament sections are typically Plummer-like (Malinen et al., 2012). This dictates a plausible, idealized initial embedded cluster to be a highly compact Plummer sphere with $r_h(0) \lesssim 0.3$ pc. Indeed, the embedded associations in the solar neighborhood (Lada & Lada, 2003; Tapia et al., 2011, 2014) and near embedded young clusters, e.g., RCW 38 (DeRose et al., 2009; Kuhn et al., 2014) and the ONC (Kroupa et al., 2001) are all found to have half mass radii well less than a parsec.

In an independent and semi-analytic study, Marks & Kroupa (2012) have investigated the initial conditions of star clusters that would give rise to the currently observed binary period distribution in several observed clusters. Here, the “inverse dynamical population synthesis” (Kroupa, 1995a) is used to infer the initial stellar density (and hence the size) of a given cluster, which would dynamically evolve an initial universal primordial binary period distribution (Kroupa, 1995a,b) to the present-day distribution. This study relates the birth mass and the half mass radius of a star cluster as,

$$\frac{r_h(0)}{\text{pc}} = 0.10^{+0.07}_{-0.04} \times \left(\frac{M_{cl}(0)}{M_\odot} \right)^{0.13 \pm 0.04}. \quad (9)$$

This gives comparable initial (embedded) cluster size as above which depends weakly on the initial mass.

The observed values of SFE in star forming clouds and embedded associations ranges widely, from less than a percent (Rathborne et al., 2014) to $\approx 30\%$ for the embedded stellar associations in the solar neighborhood (Lada & Lada, 2003). An appropriate value of SFE is even more unclear from theoretical studies which depends on a number of assumptions and inputs that are adopted in the hydrodynamic calculations. SPH calculations with spherical (or cubical) gas clouds of $< 100 - 1000s M_\odot$ without any implementation for stellar feedback, as often

done for such masses (*e.g.*, Klessen et al. 1998; Bate & Bonnell 2004; Bate 2009; Girichidis et al. 2011), cannot infer any SFE and would eventually let all of the gas be absorbed into the proto-stars (or sink particles), *i.e.*, give $\approx 100\%$ SFE as an artifact. Self regulation by stellar matter outflow (wind and jet) and radiation (Adams & Fatuzzo, 1996) is crucial to arrive at a realistic SFE. Current state-of-the-art SPH studies (reaching opacity limit and sub-sink-particle resolution) in this direction incorporate seed magnetic field in the star-forming gas and diffusive radiation feedback but are limited to individual proto-stars' scale. Proto-stars or sink particles are found to form with jet outflows where a self-regulated SFE upto $\approx 30\%$ is obtained (Bate et al. 2014; see also Machida & Matsumoto 2012). Recently, an independent analytical study (Banerjee, 2014) of formation of clump-cores (that would eventually turn into proto-stars) in gas clumps and of the maximum mass of the cores infers an upper limit of $\approx 30\%$ for the clump SFE. This is consistent with the hydrodynamic calculations with self-regulation and observations in the solar neighborhood (see above). From their SPH calculations of low-resolution but real-sized ($10^5 - 10^6 M_\odot$) turbulent molecular clouds, that include radiative feedback but no magnetic field, Dale et al. (2015), however, find high SFE approaching 100%. This inferred SFE is likely to be an overestimate due to introduction of too low resolution (where a sink particle represents a stellar sub-cluster) and partial feedback by excluding magnetic field. From this viewpoint, the outcome of the proto-star-scale calculations, as mentioned above, are much more reliable. Pfalzner & Kaczmarek (2013) also find that $\approx 30\%$ SFE best describes the age-mass and age-size correlation in young clusters of < 20 Myr age. It is, therefore, plausible but not entirely obvious to assume that the massive clusters form with the highest possible SFE, an estimate of which is $\varepsilon \approx 30\%$, according to the above mentioned studies. Note that this SFE refers to the clump (*i.e.*, over the spatial scale of a newborn cluster) efficiency; the SFE over an entire GMC is only a few percent.

The values of the timescales governing the gas expulsion timescale, *viz.*, τ_g and τ_d depend on the complex physics of gas-radiation interaction. When the gas starts to escape, it should be ionized by the UV radiation from the massive stars causing efficient coupling of the stellar radiation with the gas which is one of the primary drivers of the gas. Hence, one can plausibly use an average gas velocity of $v_g \approx 10 \text{ km s}^{-1}$ which is the sound-speed in ionized hydrogen (HII) gas. For massive clusters, whose escape speed (of the stellar system) exceeds the above v_g , the coupling of stellar radiation with the ionized gas over-pressures the latter and can even make it radiation pressure dominated (RPD) for massive enough clusters. During such RPD phase, the gas is driven at speeds well exceeding its sound-speed (Krumholz & Matzner, 2009). Once the expanding gas becomes gas pressure dominated (GPD), the outflow continues with the HII sound speed (Hills, 1980). Hence, τ_g as determined by $v_g \approx 10 \text{ km s}^{-1}$, is an *upper limit*; it can be shorter depending on the duration of the RPD state. Note that this initial RPD phase is crucial to launch the gas from massive stellar systems whose escape speed exceeds the HII sound speed (Krumholz & Matzner, 2009).

As for the delay-time, a widely used representative value is $\tau_d \approx 0.6 \text{ Myr}$ (Kroupa et al., 2001). The correct value of τ_d is again complicated by radiative gas physics.

Although stellar input to the parent gas has been studied in some detail for single low mass proto-stars (Bate et al., 2014), the phenomena is much less understood over the global scale of a massive cluster. Nevertheless, an idea of τ_d can be obtained from the lifetimes of Ultra Compact HII (UCHII) regions which can be up to $\approx 10^5$ yr (0.1 Myr; Churchwell 2002). The highly compact pre-gas-expulsion clusters (see above) are a factor of $\approx 3 - 4$ larger in size ($r_h(0)$) than a typical UCHII region (≈ 0.1 pc). If one applies a similar Strömgren sphere expansion scenario (see Churchwell 2002 and references therein) to the compact embedded cluster, the estimated delay-time, τ_d , before a sphere of radius $r_h(0)$ becomes ionized, would also be larger by a similar factor and close to the above representative value. Once ionized (*i.e.*, becomes HII from its predominantly neutral molecular or HI state), the gas couples efficiently with the stellar radiation and launched immediately (see above). High-velocity jet outflows from proto-stars (Patel et al., 2005) aid the gas outflow.

For super-massive clusters ($> 10^6 M_\odot$), *i.e.*, for proto-globular clusters, however, a “stagnation radius” can form within the embedded cluster inside which the radiation cooling becomes sufficiently efficient to possibly form second-generation stars (Wünsch et al., 2011). Also, as discussed above, the gas-outflow can initially be supersonic which generates shock-fronts. Although shocked, it is unlikely that star formation will occur in such a RPD gas. Later, during the GPD outflow, the flow can still be supersonic in the rarer/colder outer parts of the embedded cluster where the sound speed might be lower than that typical for HII gas. It is, however, unclear whether the cooling in the shocked outer regions would be efficient enough to form stars.

Admittedly, the above arguments do not include complications such as unusual morphologies of UCHIIs and possibly non-spherical ionization front, among others, and only provide basic estimates of the gas-removal timescales. Observationally, Galactic ≈ 1 Myr old gas-free young clusters such as the ONC and the HD97950 imply that the embedded phase is $\tau_d < 1$ Myr for massive clusters. The above popularly used gas-expulsion model does capture the essential dynamical response of the star cluster.

The stellar mass function of the embedded clusters is typically taken to be canonical (Kroupa, 2001). Note that the stellar entities here are proto-stars which are yet to reach their hydrogen-burning main sequences. Also, the interplay between gas accretion and dynamical processes (ejections, mergers) in the compact embedded cluster continue to shape the global stellar IMF of the cluster (Klessen et al., 1998). This IMF is often observed to be canonical for VYMCs. This gas accretion and the dynamical processes only influence the massive tail of the IMF and also sets the maximum stellar mass (Weidner & Kroupa, 2004; Weidner et al., 2013a), as indicated in hydrodynamic calculations (Klessen et al., 1998; Dib et al., 2007; Girichidis et al., 2011). The overall canonical shape of the IMF as determined by the low mass stars, which contribute to most of the stellar mass of the system ($> 90\%$), appears primarily due to gravitational fragmentation alone. There are observational evidences available which suggest that VYMCs possess a canonical IMF below $1 M_\odot$ (Shin & Kim, 2015). This justifies the adoption of the canonical IMF for the embedded (proto-) star cluster. In more recent studies (*e.g.*, Banerjee & Kroupa 2013,

2014 discussed below) an “optimal sampling” of the canonical IMF is used (Kroupa et al., 2013) which automatically terminates the IMF at the maximum stellar mass (Weidner & Kroupa, 2004).

On a separate note, efficient gas expulsion from star clusters is indirectly supported by the lack of gas in young and intermediate-aged clusters, in general. In particular, a recent survey of the LMC’s massive star clusters over wide ranges of mass ($> 10^4 M_\odot$) and age (30-300 Myr) has failed to identify reserved gas in any of these clusters (Bastian & Strader, 2014). These clusters would have accreted enough surrounding gas by now for the latter to be detected within them. This implies that star clusters can, in fact, disperse their gaseous component efficiently at any age < 300 Myr and irrespective of their escape velocities (Bastian & Strader, 2014). However, short (< 1 Myr) bursts of new star formation episodes can lead to long-term continued growth of star clusters as these may accrete gas episodically from the surrounding interstellar medium (Pflamm-Altenburg & Kroupa, 2009).

2.3 Matchings with individual very young massive clusters

The best way to validate the monolithic or episodic scenario of VYMC formation is to compare its computed outcome with the details of well observed VYMCs. There are only a few VYMCs whose profiles are measured from their centers to their halos using ground (primarily the *Very Large Telescope* or VLT) and space based (the *Hubble Space Telescope* or HST) photometry. To obtain a radial mass density profile of a dense assembly, proximity is essential as much as low extinction. This allows reliable estimates of starcounts in well resolved annuli and also the estimates of the individual stellar masses. Thus (surface) mass density profiles have been obtained only for nearby and kpc-distance Galactic young clusters. The stellar velocity dispersion in a young cluster’s central region can also constrain its initial conditions. The (one-dimensional) velocity dispersion can be obtained from stellar radial velocities from multi-epoch spectroscopy. Proper motions of the individual stars, as obtained from multi-epoch high-resolution imaging with sufficient time baseline, can provide the dispersion in the transverse velocity components. The Galactic NGC 3603 young cluster or HD97950, being our nearest starburst cluster, is perhaps the best observed VYMC whose mass density profile (obtained using the VLT; Harayama et al. 2008) and transverse stellar velocity dispersions (obtained using HST with a 10 year baseline; Rochau et al. 2010; Pang et al. 2013) are known out to ≈ 3 pc with reasonable accuracy. Being as young as ≈ 1 Myr (Stolte et al., 2004) despite being a gas free cluster, HD97950 acts as a “smoking gun” of formation of massive star clusters.

Table 1 shows model N-body computations in the literature and their corresponding parameters which have reproduced well observed VYMCs (see Table 2) beginning from single-cluster initial conditions. The key results from these works will be discussed below. All these studies utilize certain common properties and conditions as below:

Table 1 Initial and gas expulsion parameters, for the computed models beginning with monolithic initial conditions, that reproduce well observed very young massive clusters (see Sec. 2.3). See text for the meanings of the notations.

Model cluster	$M_{cl}(0)/M_{\odot}$	$M_g(0)/M_{\odot}$	$r_h(0)/\text{pc}$	τ_g/Myr	$\tau_{cr}(0)/\text{Myr}$	τ_d/Myr	$f_{\text{bin}}(0)$	Z/Z_{\odot}	Reference
ONC-B	4.2×10^3	8.4×10^3	0.21	0.021	0.066	0.6	1.0	1.0	Kroupa et al. (2001)
R136	1.0×10^5	2.0×10^5	0.45	0.045	0.021	0.6	0.0	0.5	Banerjee & Kroupa (2013)
HD97950s	1.0×10^4	2.0×10^4	0.25	0.025	0.029	0.6	0.0	1.0	Banerjee & Kroupa (2014)
HD97950b	1.0×10^4	2.0×10^4	0.25	0.025	0.025	0.6	1.0	1.0	Banerjee & Kroupa (2014)
ONC-A ^a	3.7×10^3	7.4×10^3	0.45	0.045	0.23	0.6	0.0	1.0	Kroupa et al. (2001)
NYC ^a	1.3×10^4	2.6×10^4	0.34	0.034	0.038	0.6	0.0	1.0	Banerjee & Kroupa (2013)

The initial gas mass $M_g(0)$ and the gas expulsion timescale τ_g (see Sec. 2.2) are determined by $\varepsilon \approx 0.33$ and $v_g \approx 10 \text{ km s}^{-1}$ ($\tau_g = r_h(0)/v_g$) respectively and $\tau_d \approx 0.6 \text{ Myr}$ for all these computed models. The models HD97950s/b refer to the ones with initial single-only stars/primordial binaries as computed in Banerjee & Kroupa (2014).

^a These computed models are not “matching” models but are discussed various in places of this chapter.

- The SFE $\varepsilon \approx 0.3$ and the gas dispersal is determined by $v_g \approx 10 \text{ km s}^{-1}$ ($\tau_g/\text{Myr} = (r_h(0)/\text{pc})/10$) and $\tau_d \approx 0.6 \text{ Myr}$.
- The initial stellar and gas distribution follow the same Plummer profile.

As discussed in Sec. 2.2.1, these values and conditions are representatives and idealizations but physically motivated from what we know so far from observations and calculations at smaller scales. Furthermore, in several of them (Kroupa et al., 2001; Banerjee & Kroupa, 2014) a primordial binary population is used according to the “birth period distribution” (Kroupa, 1995b; Marks et al., 2014). While it is more compute intensive, introducing primordial binaries is more realistic in light of the high multiplicity of PMS stars. In these cases, a 100% primordial binary fraction ($f_{\text{bin}}(0) = 1.0$) is used at $t = 0$ (Kroupa, 1995a). The orbital period (P) distribution of such binary population spans over a wide range, between $1.0 < \log P < 8.43$ where P is in days (Kroupa, 1995b). The binary eccentricities, e , are taken to be thermalized, *i.e.*, distributed as $f(e) \propto e$ (Spitzer, 1987). With the dynamical evolution (and also due to the orbital evolution by tidal interaction among PMS stars or the “eigenevolution”; Kroupa 1995b) of the binary population and eventual disruption of the parent cluster (by the Galactic tidal field), such a primordial binary population naturally transforms to the log-normal period distribution observed for low mass stellar binaries in the solar neighborhood (Kroupa, 1995a). A detailed discussion of the period distribution of primordial binaries, which is currently a widely debated topic (Kroupa et al., 2013; Marks et al., 2014; Leigh et al., 2015), is beyond the scope of this text.

These studies also incorporate stellar evolution and the associated mass loss in the N-body calculations using the semi-analytic BSE stellar evolution code (Hurley et al., 2000). The BSE, while available as standalone, is integrated with the NBODY6 direct N-body code (Aarseth, 2003). NBODY6 is currently the most realistic way to associate stellar (and binary) evolution with dynamics. In the following, we discuss

Table 2 Properties of VYMCs, discussed in this chapter, as inferred from observations. “—” implies that the corresponding value or quantity is ambiguous or unknown. The surface profiles known for these clusters (last column) are either stellar number or mass density profiles or both (see below).

Cluster Name	Cluster mass (M_{cl}/M_{\odot})	Age (t/Myr)	Galactocentric distance (R_G/kpc)	Half-light radius (r_h/pc)	Radial profile
ONC	$\approx 10^5$	1-2	\approx solar	—	number
R136	$\approx 10^5$	2-3	—	$\lesssim 1$	—
NGC 3603	$(1.0 - 1.6) \times 10^4$	≈ 1	\approx solar	≈ 0.75	number/mass

the key results from the studies mentioned in Table 1. For more details the reader is suggested to consult the respective references.

2.3.1 The Orion Nebula Cluster: structure and kinematics

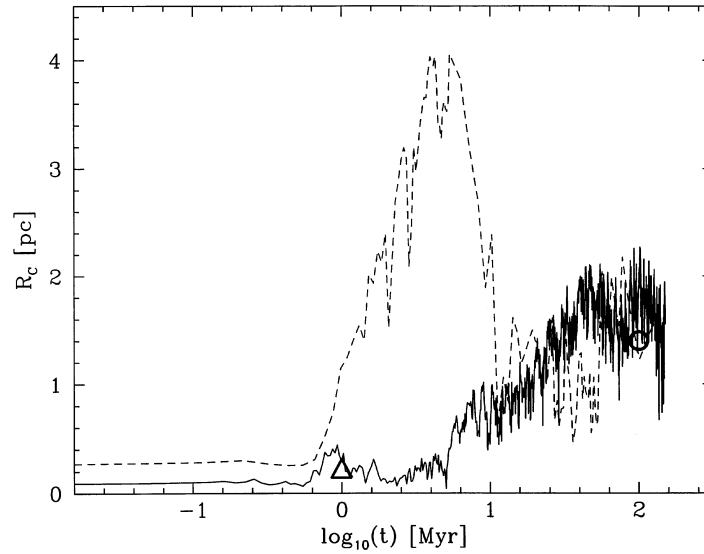


Fig. 5 The evolution of the core radius, r_c , in the ONC A (dashed curve) and the ONC B (solid curve) model clusters as computed by Kroupa et al. (2001). The open triangle and circle are the observed values of core radius for ONC (Hillenbrand & Hartmann, 1998) and Pleiades (Radboud & Mermilliod, 1998) respectively. This figure is reproduced from Kroupa et al. (2001).

Kroupa et al. (2001) provide a comprehensive study of the Orion’s main central cluster (the ONC). These authors demonstrate that an appropriate monolithic initial state with the above parameters (Table 1) well reproduce the key observed properties of the ONC. An important corollary of this work is that the ONC would dynamically evolve to a cluster similar to Pleiades in ≈ 100 Myr. Hence, a young system like the ONC represents the infant stage of an intermediate age open cluster like the

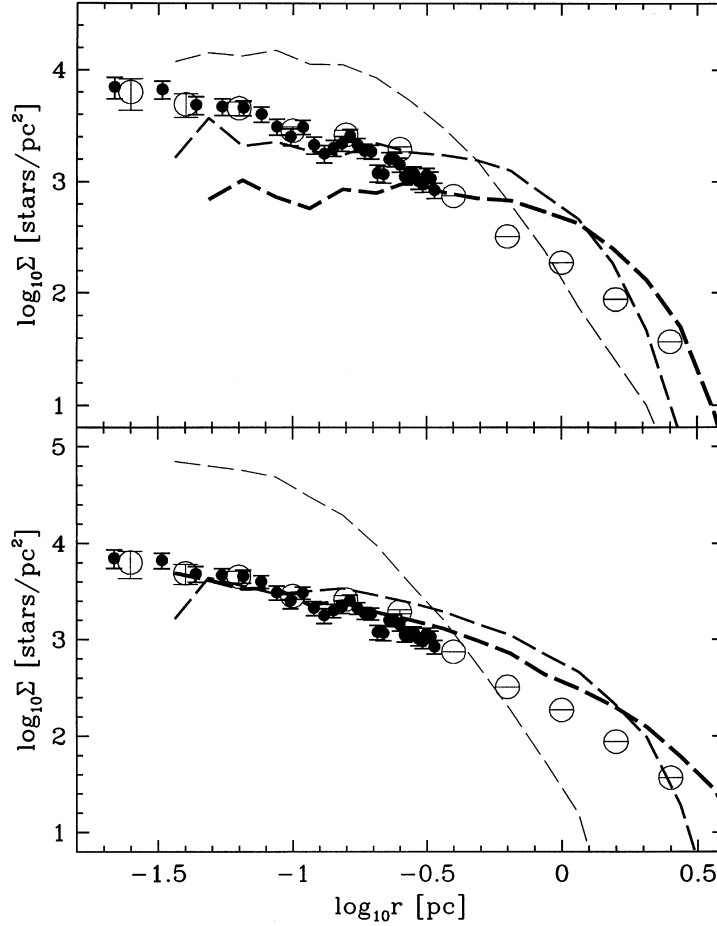


Fig. 6 The projected radial stellar number density profile at $t=0, 0.87$ and 1.1 Myr (in increasing thickness) for the computed clusters ONC A (top) and B (bottom). The open circles are observed data from Hillenbrand (1997) and the solid circles are from McCaughrean (private communication). This figure is reproduced from Kroupa et al. (2001).

Pleiades. These calculations are done using a version of the NBODY6 code that includes an analytic time-varying external gas potentials (the GASEX; Kroupa et al. 2001) as discussed above. A realistic birth primordial binary population with 100% binary fraction is used in these calculations.

Fig. 5 shows that the evolution of the core radius, r_c , for the computed models ONC-A and -B (Table 1). ONC-B agrees well with the observed r_c for the ONC at $t \approx 1$ Myr age and evolves over to be agreeable with the observed value for Pleiades at $t \approx 100$ Myr. The core-radius evolution of ONC-A, on the other hand, is far less consistent with these observed values.

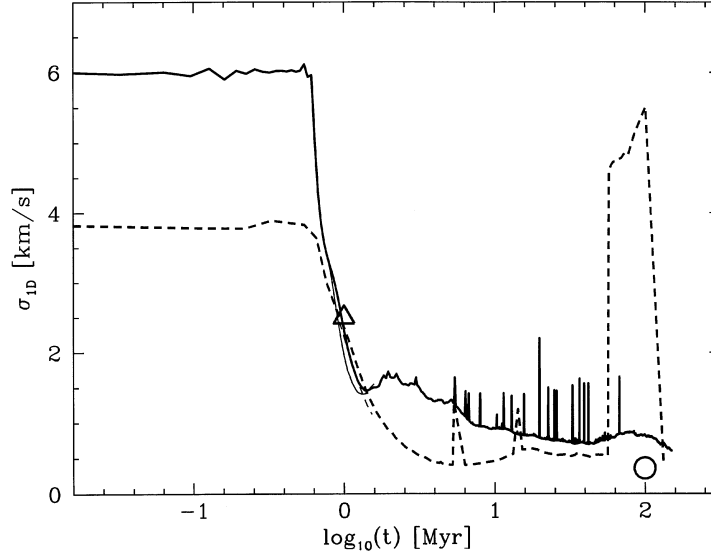


Fig. 7 The velocity dispersion of systems within $R \leq 3.2$ pc (thick curves) and within $R \leq 2.5$ pc (thin curves). The value for the Pleiades is the open circle (Radboud & Mermilliod, 1998), and the triangle is that for the ONC (Jones & Walker, 1988). The dashed and the solid lines are for ONC-A and B models respectively. The vertical excursions at later times are due to energetic binary-star encounters, which eject stars. This figure is reproduced from Kroupa et al. (2001).

Notably, model B expands to much larger extent at later times than immediately after its gas expulsion. Such late-time expansion is common for clusters with a mass spectrum and hard primordial binaries. This is driven by the mass loss due to the supernovae of the massive stars that segregate to the cluster’s central region by then. The expansion is further assisted by frequent single star-binary close encounters in the cluster’s central region that cause ejections of single and binary stars (Banerjee et al., 2012a; Oh et al., 2014) in super-elastic encounters (Heggie, 1975; Hills, 1975)⁷. This boosts the internal K.E. of the cluster’s core due to the associated mass loss and encounter recoils. The dynamical heating becomes efficient at late times after the bound fraction of the initial system re-virializes (see beginning of Sec. 2) and the most massive stars and the binaries segregate towards the cluster’s center, augmenting their density and hence the encounter rates therein. The evolutionary course of model A is however different where the initial expansion due to gas expulsion is more extensive. Being of lower mass and an initially larger radius, model A has

⁷ According to “Heggie-Hills law”, a hard binary (*i.e.*, a binary whose orbital velocity is higher than the relative velocity of its COM and the intruder) statistically becomes harder, *i.e.*, gains binding energy, in a gravitational encounter with a third body. Hence, due to energy conservation, a hard binary-single encounter would cause gain in the COM energy of the recoiling entities in the cost of deepening the binary’s potential well. This, in turn, results in an increase of the K.E. in a packed-enough environment, *e.g.*, the central region of a massive star cluster. Close encounters can result in the escape of one or both systems if they recoil exceeding the escape velocity.

lower stellar density and hence less efficient violent relaxation throughout its violent expansion phase (see beginning of Sec. 2), allowing it to expand to larger radii and cause the bound fraction to take longer to fall back (*c.f.* dashed line in Fig. 5). The longer duration of expansion and re-collapse covers a good part of the supernova phase ($t \gtrsim 3$ Myr) and makes binary-single/binary-binary encounters much less frequent. Note that for both models, the primordial binaries and the stars of all masses are distributed initially without any spatial preference, *i.e.*, without any primordial mass segregation. Also, see Sec. 2.3.2.

Fig. 6 shows the computed evolutions of the stellar (surface) number-density profiles. Being consistent with the core-radius evolution, the radial profile for the ONC-B model agrees reasonably with the observed radial stellar density profile of the ONC, out to ≈ 3 pc from the center, at $t \approx 1$ Myr (bottom panel). This is unlike the ONC-A model which is either too dense or too expanded compared to the observed radial profile (top panel).

The evolution of computed one-dimensional velocity dispersion, σ_{1d} , is shown in Fig. 7. The frequent abrupt jumps in the computed σ_{1d} at late times is due to binary-single star close encounters which cause ejections of single and binary systems from the cluster. The recoil K.E. in the encounter and the mass loss due to the escape heats up the cluster's core (see above). The long term boost in σ_{1d} for the ONC-A model between 60 - 100 Myr is an artifact of the method in which σ_{1d} is evaluated in this study which considers only binaries as centers of mass (COMs) but not higher multiplets. The increased σ_{1d} here is caused due to the outer member of a long-lasting triple system that can appear in relatively low density systems. Given that the excursions in σ_{1d} is probabilistic in nature, both A and B models are consistent with the observed values for ONC and Pleiades (*c.f.* Fig. 7).

Given the overall consistent agreement with the observed core radius, radial stellar density profile and one-dimensional velocity dispersion, ONC-B's initial conditions and parameters (Table 1) comprise an appropriate initial state of the ONC. In other words, this model represents a monolithic "solution" of the ONC. It justifies the in-situ formation of this VYMC from a single, initially bound stellar association formed in a starburst in a molecular-gas clump, after expelling the majority of the clump's gas ($\approx 70\%$ by mass). As a corollary, an ONC-like young star cluster would evolve and expand to a Pleiades-like open cluster as the above calculations show.

2.3.2 The Tarantula cluster (R136): central velocity dispersion

A common criticism put forward against the role of gas expulsion in the formation of VYMCs is the inferred dynamical equilibrium in several VYMCs. The central R136 cluster of the Tarantula Nebula of the LMC is particularly cited in this context (Hénault-Brunet et al., 2012). The inferred total photometric mass of this cluster is $\approx 10^5 M_\odot$ (Crowther, 2010) and the age of the bulk of its stars is ≈ 3 Myr (Andersen et al., 2009). Clearly, R136 is quite an outlier by mass in the high side among the well-studied nearby VYMCs (it is also at least twice as massive compared to the Arches cluster).

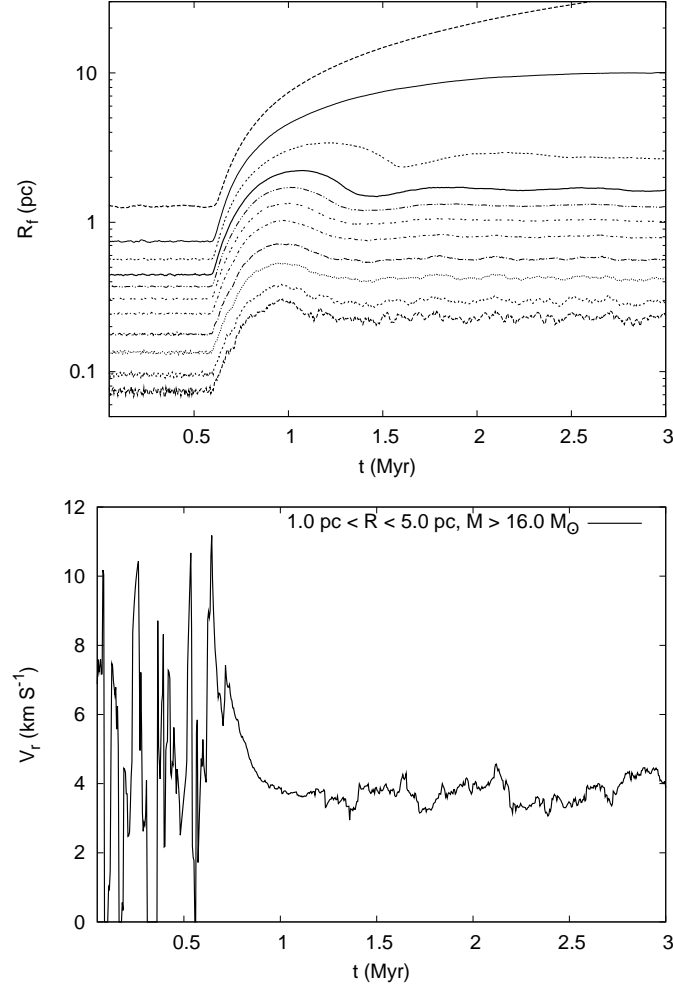


Fig. 8 Top: The evolution of the Lagrange radii, R_f , for stellar cluster mass fractions f for the computed R136 model in Banerjee & Kroupa (2013) (see Table 1). The curves, from bottom to top, correspond to $f = 0.01, 0.02, 0.05, 0.1, 0.2, 0.3, 0.4, 0.5, 0.625, 0.7$ and 0.9 respectively. The thick solid line is therefore the half mass radius of the cluster. **Bottom:** The corresponding evolution of the radial velocity (RV) dispersion, V_r , of the O-stars ($M > 16M_\odot$), within the projected distances $1 \text{ pc} < R < 5 \text{ pc}$ from the cluster center. These panels are reproduced from Banerjee & Kroupa (2013).

As a part of the ongoing “VLT-FLAMES Tarantula Survey” (VFTS; Evans et al. 2011), Hénault-Brunet et al. (2012) measured radial/line-of-sight velocities (RV) of *single* O-stars within $1 \text{ pc} \lesssim R \lesssim 5 \text{ pc}$ projected distance from R136’s center. (Strictly, the distances were measured from the most massive cluster member star R136a1. The exact location of the R136’s true density center being unknown, we consider this star be expectedly very close to the cluster’s density center.) They conclude that the RV dispersion, V_r , of the *single* O-stars within this region is $4 \text{ km s}^{-1} \lesssim V_r \lesssim 5 \text{ km s}^{-1}$. Spectroscopy (with FLAMES) at multiple epochs have been used to eliminate the radial velocities of spectroscopic binaries (Hénault-Brunet et al., 2012), *i.e.*, the above V_r corresponds the COM motion of the stars (and binaries) over the selected region of the cluster. Given the mass of R136, the above V_r is consistent with the cluster being in dynamical equilibrium at the present day.

This is contradictory to the generally accepted notion that young clusters, if emerged from recent gas dispersal, should presently be expanding. This is indeed the case for the ONC (Kroupa et al., 2001). Brandner (2008) demonstrated that young systems show an overall increase in size with age. As noted above (Secs. 1 and 2), a recently gas-expelled cluster may or may not be in dynamical equilibrium at a given age depending on the effectiveness of violent relaxation in its expanding phase. This, in turn, depends on its initial density. Hence, if initially massive and/or compact enough, a VYMC can as well be in dynamical equilibrium at present even after undergoing a significant amount of gas expulsion.

Fig. 8 (top panel) shows the evolution of the Lagrange radii for a model of a R136-like massive cluster ($M_{cl}(0) \approx 10^5 M_\odot$), *viz.*, model “R136” in Table 1. The initial half-mass radius, $r_h(0) = 0.45 \text{ pc}$, is chosen according to Eqn. 9 which is consistent with the size of embedded clusters and that of the sections of dense filaments in molecular gas clouds (see Sec. 2.2.1). These Lagrange radii (escaping and bound stars are always included) imply that the R136 cluster, under reasonable conditions (see Sec. 2.2.1), would re-virialize well within its current age of 3 Myr. The re-virialization time, in this case, is $\tau_{vir} \approx 1 \text{ Myr}$ and the bound fraction after re-virialization is $F_b \approx 0.6$, implying an efficient violent relaxation phase. This calculation (as well the following one described in this subsection) is done using the NBODY6 code (see above). No primordial binaries are used in these calculations as τ_{vir} and F_b would not get affected by binaries significantly. Also, primordial binaries are a significant computational hurdle for direct N-body calculations for such massive clusters (even for Monte Carlo calculations; *c.f.* Leigh et al. 2015).

As expected, the corresponding computed $V_r \approx 4.5 \text{ km s}^{-1}$ between 1 - 3 Myr age, as appropriate for the remaining bound virialized cluster, is consistent with the observed value for R136 (see above). This is shown in Fig. 8 (bottom panel). Note that in Fig. 8, the computed evolution of V_r corresponds to stars with (zero-age) mass $> 16 M_\odot$ which correspond to O-type stars that are used to determine the radial velocity dispersion in R136 by Hénault-Brunet et al. (2012). Also, V_r is computed within $1 \text{ pc} \lesssim R \lesssim 5 \text{ pc}$ as observed by the above authors. The initial large fluctuations in V_r for $\tau_d < 0.6 \text{ Myr}$ are due to the initial mass-segregated condition used in this calculation (Banerjee & Kroupa, 2013), which results in only a few O-stars

$$\tau_{\text{seg}} \approx 15 \frac{\langle m \rangle}{m_{\text{massive}}} \tau_{\text{rh}}(0), \quad (10)$$

Fig. 9 shows the Lagrange radii of a computed model that is a few factors less massive than the R136 model discussed above. This model corresponds to the NBODY6-computed model “NYC” in Table 1 whose mass is similar to the NGC 3603 Young Cluster (HD97950). Note that while this model is not a “matching model” for NGC 3603 cluster which are covered in the following subsection (models “HD97950”s/b of Table 1), the initial conditions are similar. Unlike the R136 model, the re-virialization time is much longer in this case, *viz.*, $\tau_{\text{vir}} \approx 2$ Myr. Hence at its present age of ≈ 1 Myr, an NGC3603-like young cluster would not be in dynamical equilibrium (except in its innermost regions; see Sec. 2.3.3), as one generally expects. As discussed in Sec. 2.3.1, a smaller $M_{cl}(0)$ and hence less initial stellar density causes the NYC model to take longer to regain dynamical equilibrium with a reduced bound fraction ($F_b \approx 0.3$).

From the above calculations it can be said that “an observed dynamical equilibrium state of a very young stellar cluster does not necessarily dictate that the cluster has not undergone a substantial gas-expulsion phase” (Banerjee & Kroupa, 2013). The R136 cluster is very likely a VYMC that is promptly re-virialized after its gas expulsion owing to its large mass (hence initial density). Admittedly, these conclusions depend on the initial and gas expulsion conditions. As discussed in Banerjee & Kroupa (2013), the above conclusions are immune to reasonable variations in the gas expulsion timescales τ_d and τ_g , as long as $\varepsilon \approx 33\%$ which is reasonable for VYMCs (see Sec. 2.2.1).

In passing, it is worthwhile to consider the effect if the SFE possibly varies radially across the initial cluster (Adams, 2000). In that case, the central region of the cluster is likely to have a higher SFE due to higher density there. The resulting gas removal preferentially from the outer parts of the cluster would cause it to expand less than the corresponding case of a uniform SFE. This would, in turn, shorten τ_{vir} and increase F_b , *i.e.*, the above conclusions still remain unchanged.

2.3.3 NGC 3603 young cluster: structure and kinematics

Being our nearest starburst cluster, the central young cluster HD97950 of the Galactic NGC 3603 star-forming region is perhaps the best observed VYMC. Due to its proximity (≈ 7 kpc from the Sun) and brightness (photometric mass $10000M_\odot \lesssim M_{cl} \lesssim 20000M_\odot$) its radial stellar mass-density profile for low mass stars (Harayama et al., 2008) (using VLT observations in NIR) and the number-density profile for stars up to $100M_\odot$ (Pang et al., 2013) are determined, both out to 3 pc ($R \approx 100''$) from its center. Furthermore, its central velocity dispersion, within $R \lesssim 0.5$ pc ($\approx 15''$), and the stellar tangential velocities are determined from proper motion measurements with the HST (≈ 10 year baseline; Rochau et al. 2010; Pang et al. 2013).

In Banerjee & Kroupa (2014), a set of initial conditions is presented which remarkably reproduce the above structural and kinematic data of the HD97950 cluster, *viz.*, the models “HD97950s/b” of Table 1. These computed clusters (using NBODY6) have the same initial conditions, except that HD97950b contains a primordial binary population. This binary population is taken to be the birth population (Kroupa, 1995b), except that a uniform distribution in $\log_{10} P$ between $0.3 < \log_{10} P < 3.5$ and a mass ratio biased towards unity (ordered pairing; as introduced by Oh & Kroupa 2012) is used for stellar masses $m > 5M_\odot$. This is motivated by the observed period distribution of O-star binaries in nearby O-star rich clusters (Sana & Evans, 2011; Chini et al., 2012). It is currently unclear at which stellar mass and how the orbital period law changes and the above switching of the P -distribution at $m = 5M_\odot$, therefore, is somewhat arbitrary. Note that for this P -distribution, the primordial binaries are much tighter and hence energetic in dynamical encounters for $m > 5M_\odot$.

Both the computed models reproduce the HD97950 cluster reasonably but the one with the above primordial binary distribution (*i.e.*, HD97950b) does better in

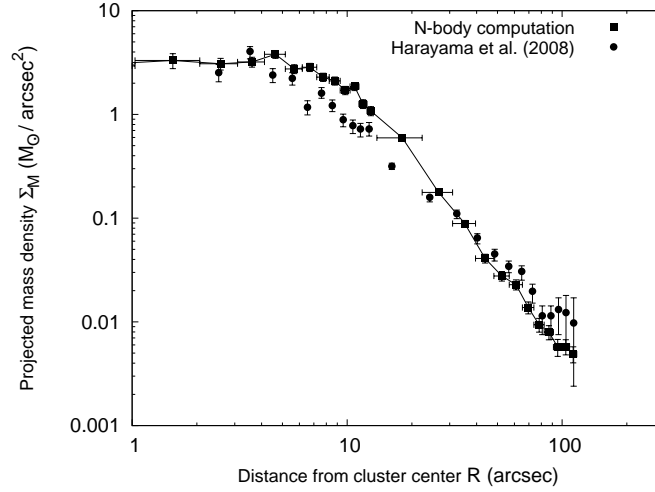


Fig. 10 The computed projected mass density profile (filled squares and solid line) for the stellar mass range $0.5M_{\odot} < m < 2.5M_{\odot}$ at $t \approx 1.4$ Myr, from the computed model HD97950b ($r_h(0) \approx 0.25$ pc, $M_{cl}(0) \approx 10000M_{\odot}$; see Table 1) containing an initial primordial binary population (see Sec. 2.3.3). This computed profile shows remarkable agreement with the observed profile (Harayama et al., 2008), for the same stellar mass range, of the central young cluster (HD97950) of NGC 3603 (filled circles). The angular annuli (the horizontal error bars) used for computing the projected densities are nearly the same as those used by Harayama et al. (2008) to obtain the observed profile. The vertical error bars are the Poisson errors for the individual annuli. This panel is reproduced from Banerjee & Kroupa (2014).

terms of matching the central velocity dispersion. A substantial fraction of tight massive binaries ($\approx 50\%$ in this case) augments the central velocity dispersion due to energetic binary-single interactions (binary heating) and makes it agree better with the observed value in this case (Banerjee & Kroupa, 2014). Here, only the HD97950b model is detailed.

Fig. 10 shows the surface or projected mass density profile Σ_M at $t \approx 1.4$ Myr for the HD97950b model (filled squares joined by solid line). It matches remarkably with the observed profile in HD97950 (filled circles; Harayama et al. 2008). Note that in this comparison a similar stellar mass range and annuli as those for the observed profile are used to construct the density profile from the computed cluster.

Fig. 11 shows the radial profile of the incompleteness-limited stellar number density Σ_N from the above computed cluster (filled squares joined by solid line) at $t \approx 1.4$ Myr and that obtained from the HST (Pang et al., 2013) (filled triangles) which agree remarkably. Here, the computed stellar distribution is sampled according to the radius and mass-dependent incompleteness fraction particular to this observation (Pang et al., 2013). This mimics the “observation” of the model cluster. Note that in constructing both of these density profiles we include only the most massive member (primary) of a binary which would dominate the detected light from it.

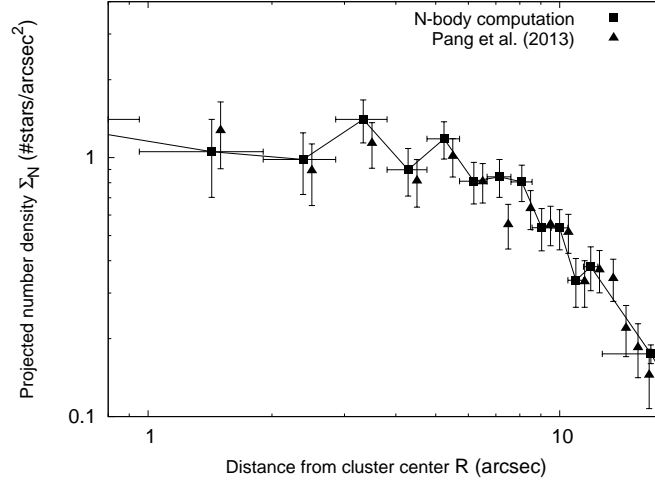


Fig. 11 The computed projected stellar number density profile for the calculation HD97950b (Table 1; filled squares and solid line). This shows a remarkable agreement at $t \approx 1.4$ Myr with the same obtained with the stars of HD97950 from the HST/PC chip (up to the central $15''$; filled triangles; chip data from Pang et al. 2013). In constructing the computed profile, the incompleteness in the detection of the stars is taken into account that depends on the stellar mass (luminosity) and projected angular annuli on the cluster, as given in Pang et al. (2013). In this comparison, similar angular annuli (horizontal error-bars) are used to construct the density profiles. The vertical error bars are the corresponding Poisson errors. This panel is reproduced from Banerjee & Kroupa (2014).

Fig. 12 (bottom) shows the evolution of the (one-dimensional) dispersion of the stellar velocity components, σ_{1d} ($1d = x, y, z$), for the HD97950b model for $1.0M_{\odot} < m < 100.0M_{\odot}$ within $R < 0.5$ pc. The computed σ_{1d} s lie between $4.0 < \sigma_{1d} < 7.0$ km s $^{-1}$ for $1 < t < 2$ Myr. The corresponding observed one-dimensional velocity dispersions indeed vary considerably with orthogonal directions (Pang et al., 2013) like the computed ones here (see Fig. 12; bottom panel) and their variation well matches the above computed range. Fig. 12 (top) shows the σ_{1d} s corresponding to the stellar mass range $1.7M_{\odot} < m < 9.0M_{\odot}$ as in Rochau et al. (2010). The corresponding mean σ_{1d} is consistent with that obtained by Rochau et al. (2010) from HST proper motions. The abrupt vertical excursions in σ_{1d} in Fig. 12 (bottom) are due to energetic two- or few-body encounters which are most frequent for the most massive stars and binaries as they centrally segregate the most via two-body relaxation.

Fig. 13 shows radial profiles of σ_{1d} , from HD97950b, at $t = 1.4$ Myr for $1.0M_{\odot} \leq m \leq 100.0M_{\odot}$. Here, σ_{1d} tends to increase for $R \gtrsim 40'' (\approx 1.2$ pc) which can be attributed to the recent gas expulsion from the system causing its outer parts to still expand. Such a trend, which becomes more pronounced the closer the epoch of observation is to the gas expulsion, can be tested by future, more accurate determinations of stellar proper motions in the outer regions of HD97950, *e.g.*, by *Gaia*.

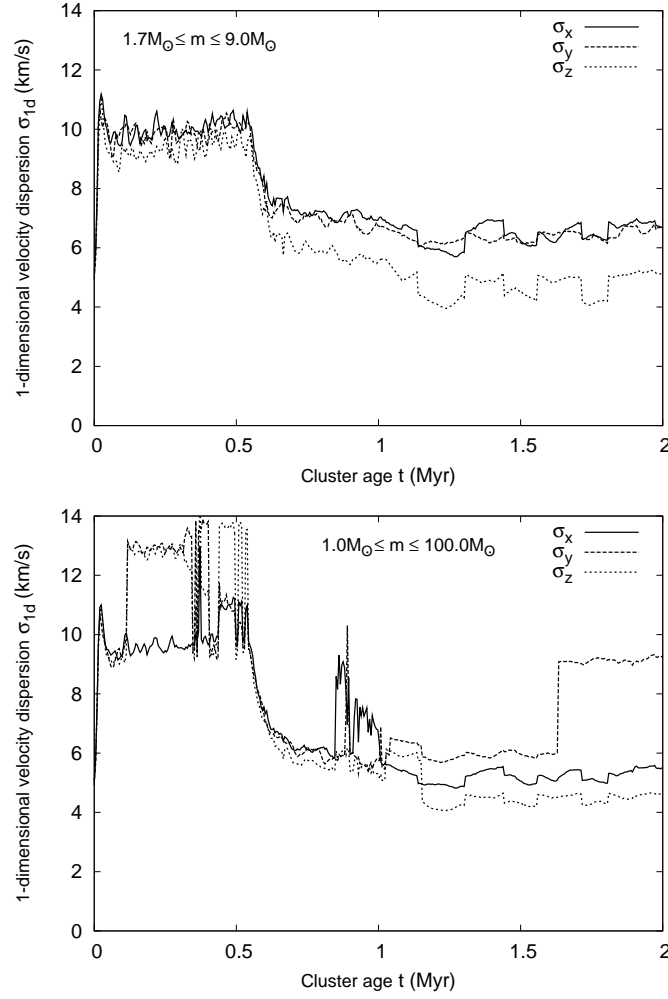


Fig. 12 The time evolution of the one-dimensional velocity dispersions, σ_{1d} s, for the model cluster HD97950b (see Table 1), the density profile of which is shown in Fig. 10. They are obtained for $R < 0.5$ pc ($\approx 15''$) and correspond to the stellar mass ranges $1.7M_{\odot} < m < 9.0M_{\odot}$ (as in Rochau et al. 2010; top panel) and $1.0M_{\odot} < m < 100.0M_{\odot}$ (as in Pang et al. 2013; bottom panel). The σ_{1d} s obtained here correspond to the COMs of the cluster single-stars and binaries. The computed values of σ_{1d} (bottom panel) differ in orthogonal directions as found in observations (Pang et al., 2013) and span the same range as observed ($4.5\text{--}7.0$ km s $^{-1}$) between 1.0 - 1.5 Myr cluster age, implying good agreement. These panels are reproduced from Banerjee & Kroupa (2014).

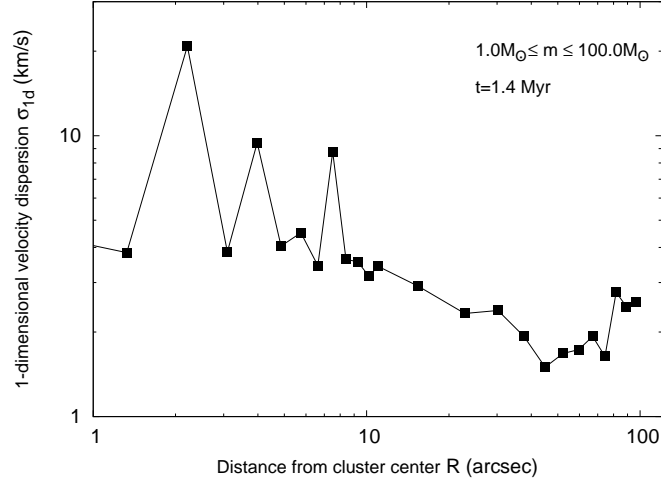


Fig. 13 Radial variation of one-dimensional velocity dispersion, σ_{1d} , for the computed HD97950b model (here in presence of a tidal field) at $t = 1.4$ Myr for stellar mass range $1.0M_{\odot} \leq m \leq 100.0M_{\odot}$. The overall increasing trend of σ_{1d} with R in the outer regions ($R \gtrsim 40''$ in this case) is due to the recent gas expulsion. The tangential velocities of selected stars in Pang et al. (2013) (for $R \lesssim 60''$) do show an increasing trend with R . This panel is reproduced from Banerjee & Kroupa (2014).

Notably, the measured tangential velocities (from HST proper motions) of selected stars in Pang et al. (2013) indeed show an increasing trend with radial distance in the outer region (measured up to $R \approx 60''$) of HD97950. Note that the inner annuli of the above computed cluster are already virialized at $t = 1.4$ Myr but the outer region is still far from re-virialization (see Fig. 1 of Banerjee & Kroupa 2014). As demonstrated in Sec. 2.3.2, the overall re-virialization time for such a cluster is $\tau_{\text{vir}} \approx 2$ Myr.

Hence, the HD97950 computed cluster well reproduces the structure and the internal kinetics of the observed HD97950 cluster. In other words, model HD97950b (also HD97950s to some extent) is a monolithic “solution” of the NGC 3603 cluster; it represents an initial stellar distribution that would evolve self consistently to make the HD97950 cluster at its appropriate age.

Initial Plummer-profiled and highly compact ($r_h(0) \approx 0.2 - 0.3$ pc) monolithic embedded clusters, when subjected to residual gas expulsion, remarkably reproduce the hitherto known kinematic and structural properties of the well observed young clusters the ONC, R136 and NGC 3603. The properties of the required gas expulsion are seemingly universal ($\varepsilon \approx 0.3$, $\tau_d \approx 0.6$ Myr and $v_g \approx 10 \text{ km s}^{-1}$). Such computed model clusters are the only ones to date that directly reproduce these observed clusters.

3 Hierarchical formation of young massive clusters: the case of NGC 3603 young cluster

Although an episodic and in-situ formation scenario is well consistent with the detailed properties of several observed Galactic or local VYMCs (Sec. 2), it is still puzzling how such smooth initial condition can be connected with irregular, substructured and/or filamentary morphology of GMCs and embedded stellar distributions (see Sec. 1). Substructures are also found in several gas-free or near gas-free very young star clusters, even though they may have an overall core-halo profile (Kuhn et al., 2014). Computations of gravitational fragmentation in turbulent gas clouds also point to a highly substructured beginning of a star cluster (see Sec. 1).

Table 3 A basic classification of the different morphologies in the spatial distribution of stars that can occur in the process of subcluster merging. These morphologies appear in the models computed here (Sec. 3). Note that the distinctions among these morphologies are only qualitative and are made for the ease of descriptions. This table is reproduced from Banerjee & Kroupa (2015).

Morphology	Abbreviation
Substructured	SUB
Core + asymmetric and/or substructured halo	CHas
Core-halo with near spherical symmetry	CH
Core + halo containing satellite clusters	CHsat

One way to “add up” these two apparently conflicting pictures of VYMC formation is indicated by the timescale problem of hierarchical formation as discussed in Sec. 2.1. Essentially, the age, density and velocity dispersion profiles of observed VYMCs well constrain the admissible initial spatial scale of any subcluster system from which the VYMC may have formed. In particular, Fig. 3 implies that substructures can appear and migrate from sufficiently close separation to possibly form a VYMC within a few Myr. Such “prompt hierarchical merging” can connect a monolithic initial condition, which successfully explains observed VYMCs (Kroupa et al., 2001; Banerjee & Kroupa, 2013, 2014) and general properties of young clusters (Pfalzner, 2009; Pfalzner & Kaczmarek, 2013), to the conditions in dense star-forming molecular regions. The detailed observed properties of the HD97950 cluster again provides a testbed for such a scenario as discussed below.

In Banerjee & Kroupa (2015), substructured initial conditions are generated by distributing compact Plummer spheres uniformly over a spherical volume of radius R_0 . The total stellar mass distributed in this way is always the lower photometric mass estimate of $M_* \approx 10^4 M_\odot$ for HD97950, as motivated by Banerjee & Kroupa (2014); see Sec. 2.3.3. This fashion of initial subclustering is an idealization and extrapolation of what is found in the largest SPH calculations of cluster formation to date (Bate, 2009, 2012; Girichidis et al., 2011) (see Sec. 1). As discussed in Sec. 2.2.1, the initial half mass radii, $r_h(0)$, of these Plummer subclusters are taken typically between 0.1-0.3 pc, in accordance with the observed widths of these highly compact molecular-cloud filaments (André et al., 2011; Schneider et al., 2012). Such

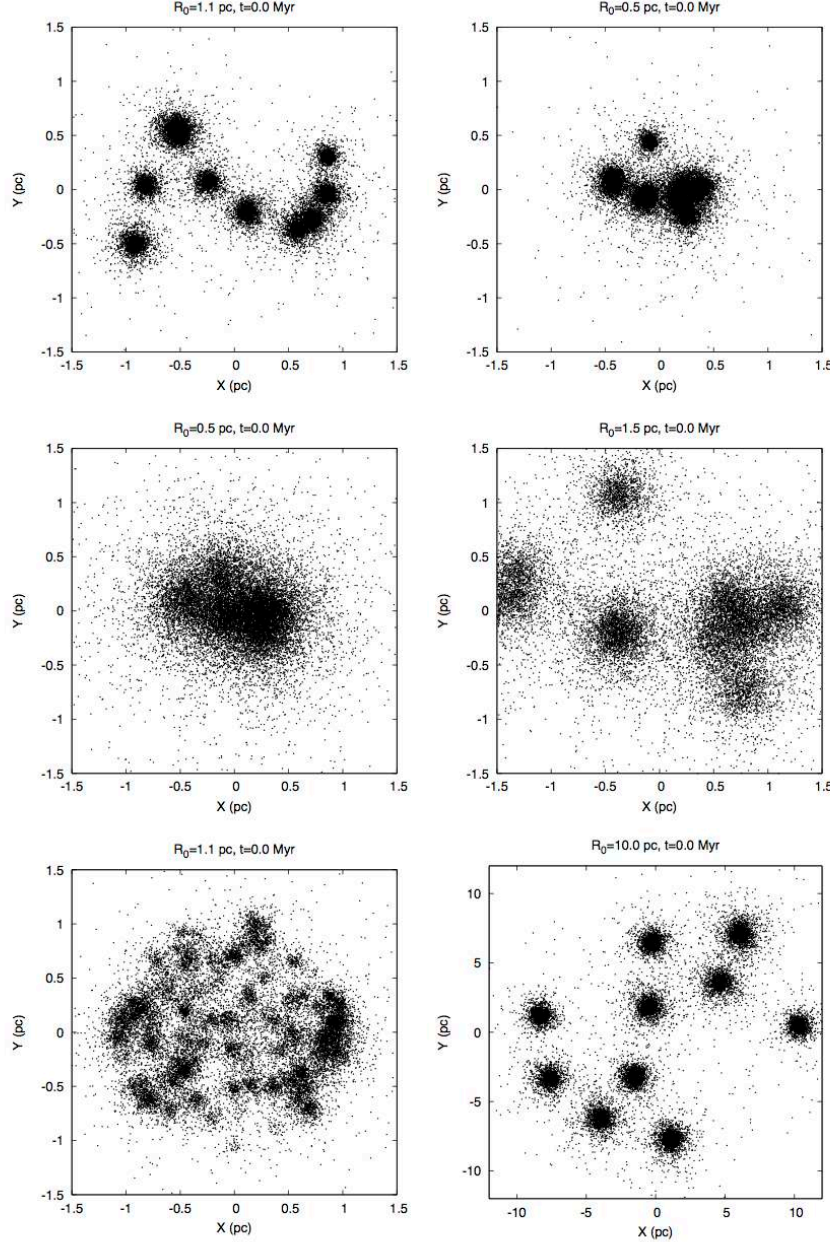


Fig. 14 The primary varieties of the *initial* configurations considered in Sec. 3, shown in projection. Here, the panels are numbered left-to-right, top-to-bottom. In each case, a set of Plummer spheres (subclusters) are uniformly distributed over a spherical volume of radius R_0 , totalling a stellar mass of $M_* \approx 10000M_\odot$. Panels 1, 2, 3, 4 and 6 are examples of type A or “blobby” systems containing 10 subclusters of $m_{cl}(0) \approx 10^3 M_\odot$ each. With smaller R_0 , the subclusters overlap more with each other (*c.f.*, panels 1 & 2 with subcluster half mass radius $r_h(0) \approx 0.1$ pc and panels 3 & 4 with $r_h(0) \approx 0.3$ pc). This is also true for increasing $r_h(0)$ (*c.f.*, panels 1 & 4). Panel 5 is an example of type B or “grainy” initial configuration containing ≈ 150 subclusters of mass range $10M_\odot \lesssim m_{cl}(0) \lesssim 100M_\odot$. While panels 1-5 are examples of “compact” configurations, for which $R_0 \leq 2.5$ pc, panel 6, with $R_0 = 10$ pc, represents an “extended” configuration where the subclusters are much more distinct. See Sec. 3 for details of the initial setups. These panels are reproduced from Banerjee & Kroupa (2015).

Table 4 An overview of the evolutionary sequences of the primary systems as computed here (Sec. 3). A particular row indicates how the morphology (see Table 3) of the corresponding system evolves with evolutionary time (in Myr as indicated by the numerical values along the columns 3-5 and 6-8), for systems both without and with a background gas potential (see text). As expected, the systems, in general, evolve from substructured to a core-halo configuration with a timescale that increases with increasing initial extent R_0 . See text for details. This table is reproduced from Banerjee & Kroupa (2015).

Config. name	Short name	Without gas potential			With gas potential ($\varepsilon \approx 0.3$)		
m1000r0.1R1.1N10 ^a	A-Ia	0.2,SUB	0.6,CHas	1.0,CH	0.2,SUB	0.6,CHas	1.0,CH
m1000r0.3R1.1N10	A-Ib	0.2,SUB	0.6,CHas	1.0,CHas	0.2,SUB	0.6,CHas	1.0,CHas
m1000r0.1R2.5N10	A-IIa	0.6,SUB	1.0,SUB	2.0,CH	0.6,SUB	1.0,CHsat	2.0,CHas
m1000r0.3R2.5N10	A-IIb	0.6,SUB	1.0,SUB	2.0,CHas	0.6,SUB	1.0,CHsat	2.0,CHas
m10-150r0.01-0.1R1.1N150 ^b	B-Ic	0.2,SUB	0.6,CHas	1.0,CH	0.2,SUB	0.6,CHas	1.0,CHas
m10-150r0.1R1.1N150	B-Ia	0.2,SUB	0.6,CHas	1.0,CH	0.2,SUB	0.6,CHas	1.0,CHas
m10-150r0.1R2.5N150	B-IIa	0.6,SUB	1.0,SUB	2.0,CHas	0.6,SUB	1.0,CHas	2.0,CHas
m1000r0.5-1.0R5.0N10	A-IIIc	1.0,SUB	2.0,SUB	3.0,CHas	1.0,CHsat	2.0,CHsat	3.0,CHsat
m1000r0.5-1.0R10.0N10	A-IVd	1.0,SUB	2.0,SUB	3.0,SUB	1.0,SUB	2.0,SUB	3.0,CHsat

^a mxyRzNn implies an initial system (at $t = 0$) comprising of $N = n$ Plummer clusters, each of mass $m = m_{cl}(0) = xM_\odot$ and half-mass radius $r = r_h(0) = y$ pc, distributed uniformly over a spherical volume of radius $R = R_0 = z$ pc.

^b Further, when a range of values $x1 - x2$ is used instead of a single value, it implies that the corresponding quantity is uniformly distributed over $[x1, x2]$ at $t = 0$.

compactness of the subclusters is also consistent with those observed in stellar complexes, *e.g.*, in the Taurus-Auriga (Palla & Stahler, 2002). However, in some calculations, larger $r_h(0)$ s are also used (see Table 4).

The number of subclusters, n , over which the $M_* \approx 10^4 M_\odot$ is subdivided has to be chosen somewhat arbitrarily. To keep a broad range of possibilities, two primary cases of the initial subdivision of the total stellar mass are considered. The “blobby” (type A) systems comprise 10 subclusters of $M_{cl}(0) \approx 10^3 M_\odot$ each. Panels 1, 2, 4 and 6 of Fig. 14 are examples of such initial systems. Note that in this and all the subsequent figures, the panels are numbered left-to-right, top-to-bottom, unless stated otherwise. The “grainy” (type B) systems comprise ≈ 150 subclusters with mass range $10M_\odot \lesssim M_{cl}(0) \lesssim 100M_\odot$ summing up to $M_* \approx 10^4 M_\odot$. The mode of initial subdivision does not influence the key inferences from these calculations.

The initial spanning radius, R_0 , is taken over a wide range, *viz.*, $0.5 \text{ pc} \lesssim R_0 \lesssim 10.0 \text{ pc}$, to explore the wide range of molecular cloud densities (see below) and spatial extents as observed in star-forming regions and stellar complexes. Table 4 provide a comprehensive list of the initial conditions for the computations in Banerjee & Kroupa (2015). The detailed nomenclature of the computed model, in its first column, is explained in Table 4 and the corresponding short names, in the second column, are self-explanatory.

As explained in Sec. 2.2.1, the proto-stellar mass function is taken to be canonical but without any upper bound. This would cause the IMF of the merged cluster, with stellar mass $M_*(\equiv M_{cl})$, also to be canonical as often observed in VYMCs. Note that the gas accretion and the dynamical processes mostly determine the massive

tail of the IMF and also sets the maximum stellar mass, m_{\max} , of the *final* cluster, as seen in hydrodynamic calculations (*e.g.*, Klessen et al. 1998; Girichidis et al. 2011). This gives rise to an $m_{\max} - M_{cl}$ relation that is consistent with that found from observations (Weidner & Kroupa, 2004; Weidner et al., 2013a). Note that if the $m_{\max} - M_{cl}$ relation applies to the pre-merger subclusters, then the $m_{\max} - M_{cl}$ relation for the final cluster will show features arising from the merging process (Weidner et al., 2010, 2013a).

All subclusters are initially at rest w.r.t. the centre of mass (COM) of the stellar system. While this condition is again an idealization, it is consistent with the results of detailed hydrodynamic computations in which the system(s) of subclusters formed is(are) typically sub-virial. Also, for the ease of computing, primordial binaries are excluded from these calculations. Test calculations show that primordial binaries do not influence the subcluster merging process significantly. The subclusters are generated using the MCLUSTER utility (Küpper et al., 2011) which is integrated in a special program that generates the overall subcluster system with the intended parameters.

The dense residual molecular cloud is represented by a background, external gravitational potential of a Plummer mass distribution which declines exponentially as discussed in Sec. 2.2. In this way the overall dynamical effect of the molecular cloud is included (as in the previous studies). In order to compare with the previous studies (Kroupa et al., 2001; Banerjee & Kroupa, 2014), we adopt a local SFE of $\varepsilon \approx 33\%$ within the span of the subclusters, R_0 . Such an SFE is as well consistent with those obtained from self-regulated hydrodynamic calculations and also with observations of embedded systems in the solar neighborhood (see Secs. 1 & 2.2.1). Hence, the geometric/density centre of the Plummer gas sphere is co-incident with the COM of the initial stellar system and its half mass radius is equal to R_0 which contain $2M_*$ mass, giving $\varepsilon = 1/3$ within R_0 . For the entire Plummer cloud (of $4M_*$), $\varepsilon = 1/5$. Inserting the adopted value $M_* = 10^4 M_\odot$ (see above), one gets $3 \times 10^4 M_\odot$ (gas + stars) within R_0 . This gives an ONC-like $\rho_g \approx 6 \times 10^3 M_\odot \text{ pc}^{-3}$ gas density for $R_0 = 1.06 \text{ pc}$ and $\approx 1/1000$ th of this for $R_0 = 10 \text{ pc}$ which is appropriate for, *e.g.*, the Taurus-Auriga complex.

3.1 General evolutionary properties of subcluster systems

As discussed in Sec. 2.1, the subclusters pass through each other for the first time at the system's potential minimum in a time t_{in} as given by Eqn. 6. The final merger of the subclusters, however, is completed after an additional violent relaxation time, t_{vrx} , which can be several subcluster orbital times. During this time, the orbital energy of the subclusters is dissipated, in multiple mutual passes, in the individual stellar orbits; this corresponds to the re-virialization process in initially monolithic systems (see Sec. 2). Both t_{in} and t_{vrx} increases with the initial span of the subclusters R_0 and hence the time for forming the final merged, (near) spherical cluster.

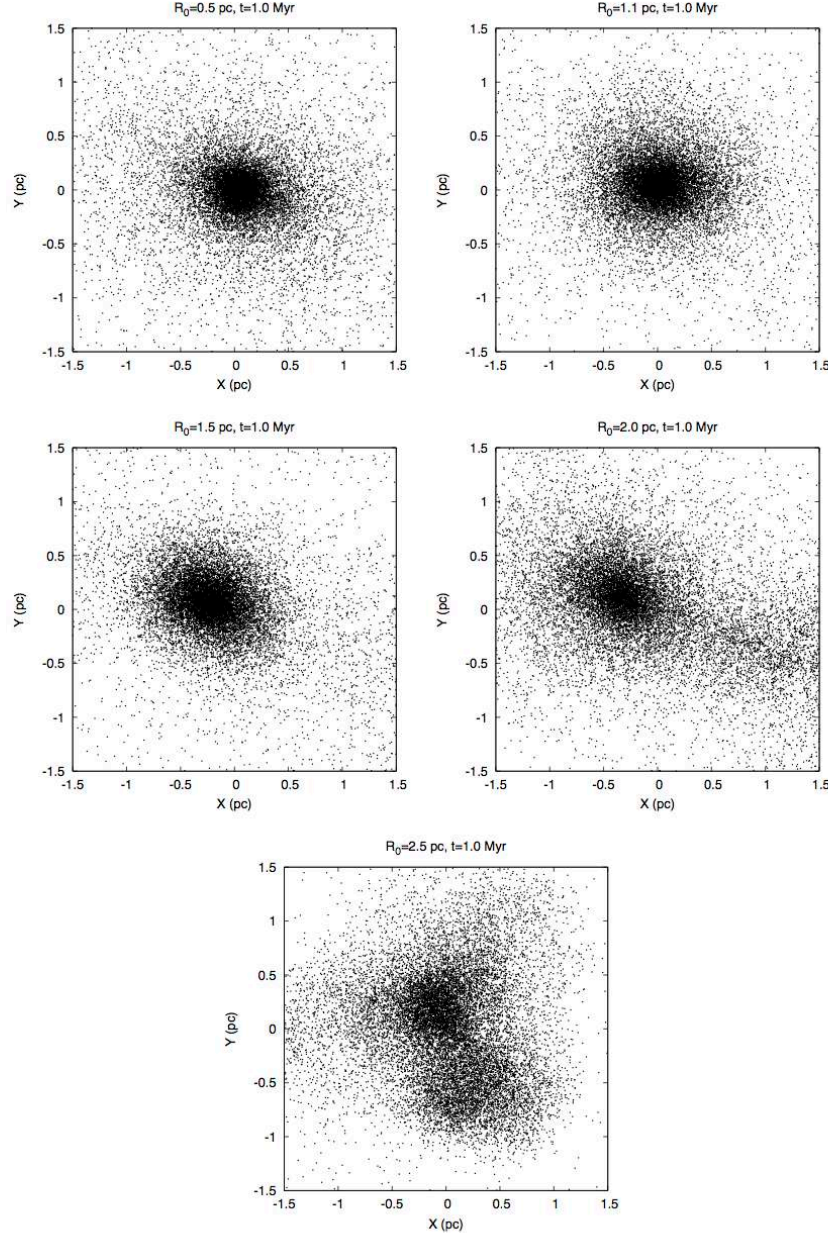


Fig. 15 Configurations obtained at $t \approx 1$ Myr with increasing initial span R_0 (without background gas potential). With increasing R_0 , the system's morphology at $t \approx 1$ Myr changes from being near-spherical core-halo (CH; panels 1,2; numbered left-to-right, top-to-bottom), asymmetric core-halo (CHas; panels 3,4) to substructured (SUB; panel 5). For $R_0 \gtrsim 2$ pc (panels 4,5), the stellar system is still well in the process of merging at $t \approx 1$ Myr after the subclusters' first pericenter crossings (*i.e.*, it is in the violent relaxation phase $t_{in} < t < t_{in} + t_{vrx}$; see Sec. 3.1). These panels are reproduced from Banerjee & Kroupa (2015).

Table 4 summarizes the evolution (in Myr) of the subcluster systems of type A and B (see above) with increasing R_0 and in presence and absence of a gas potential (see above). Only the primary templates are included here which are computed using NBODY6. For description purposes, the evolving morphology of the stellar system is divided into four categories as in Table 3. All computed configurations initiate as SUB and evolve via the intermediate CHas phase to the final CH cluster in dynamical equilibrium. $R_0 \lesssim 1$ pc systems attain a CH structure in $t \lesssim 1$ Myr without a gas potential. On the other hand, initially wider configurations remain SUB at $t = 1$ Myr even with the gas potential and most of them do not attain the CH phase even in 2 Myr. In all such calculations, a negligible fraction of stars escape the system during the infall and the merger process. In other words, the total bound stellar mass M_* remains nearly unaltered as the system evolves from SUB to CH configuration.

Fig. 15 shows the snapshots at $t \approx 1$ Myr for a set of A-type configurations (Table 4) falling from increasing R_0 (without background gas potentials). With R_0 , the morphology at 1 Myr changes from being CH, CHas to SUB. For $R_0 \gtrsim 2$ pc, the structure at 1 Myr substantially deviates from spherical symmetry (and dynamical equilibrium).

It is worth noting that due to energy conservation the size of the final cluster in dynamical equilibrium can be simply related to that of the initial subclusters (of equal or similar size and mass) as (Banerjee & Kroupa, 2015),

$$\frac{1}{2R_*} \approx \frac{1}{2nR_{cl}} + \frac{1}{R_0}. \quad (11)$$

Here, R_* is the half mass radius of the final cluster and R_{cl} is that for the initial subclusters.

The morphology of a gravitationally bound stellar population (of a given total mass) at a given age depends on the initial length scale over which the population is hatched (*i.e.*, from the mutual separation from which they fall in the resultant potential well). The dynamical timescale of the stellar population is the key in determining the morphology and length scale of the stellar distribution at the epoch of observation. A sufficiently spread-out distribution can remain highly substructured for 10s of Myr. On the other hand, a spherical massive star cluster in dynamical equilibrium can form out of a closely distributed (typically $\lesssim 2$ pc) but highly substructured stellar population in < 1 Myr.

3.2 Comparison with NGC 3603 young cluster

To assemble a HD97950-like star cluster by hierarchical merging of subclusters, the necessary but not sufficient condition is to arrive at a CH configuration in $t \lesssim 1$ Myr. The above calculations imply that to have a CH morphology at 1 Myr, one should

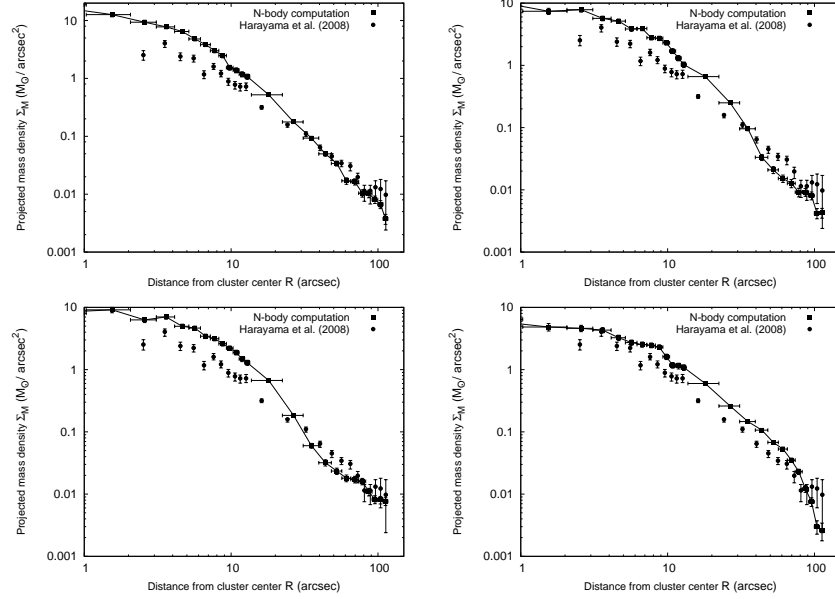


Fig. 16 Examples of surface mass-density profiles at $t \approx 1$ Myr for those computed configurations (filled squares connected with solid line) which evolve to form a star cluster with near-spherical core-halo structure (the CH-type morphology; see Table 3) within $t < 1$ Myr, in absence of a background gas potential. These computed profiles are significantly more compact and centrally overdense than that observed in HD97950 (Harayama et al. 2008; filled circles). For HD97950 $1'' \approx 0.03$ pc. This panels are reproduced from Banerjee & Kroupa (2015).

have $R_0 \lesssim 2$ pc with or without a gas potential (*c.f.* Fig. 15). As discussed in Sec. 2.1, the gas potential would actually delay the approach to a CH configuration. How does this final cluster compare with the observed HD97950 cluster?

All the configurations, *without* the gas potential, that become CH in $t \lesssim 1$ Myr are found to form clusters that are much more dense and compact compared to the observed HD97950 profile (Harayama et al., 2008) at $t \approx 1$ Myr. This is found to be true irrespective of the mode of subdivision of the initial stellar mass M_* (*c.f.* Table 4). The latter fact can be expected from Eqn. 11. This is demonstrated in Fig. 16. Note that all these calculations are for $M_* \approx 10000 M_\odot$ which is the lower mass limit of HD97950. For larger M_* , the assembled system will be even more overdense since the length scale of the final merged cluster, R_* , is nearly independent of the total stellar mass M_* (*c.f.* Eqn. 11). From test calculations, it is also found that the “heating effect” of primordial binaries and mass loss due to stellar winds do *not* expand and dilute the merged cluster’s center sufficiently.

One way to dramatically expand a star cluster, however, is to subject it to a substantial gas expulsion on a timescale of the order of its dynamical time, as discussed in the above sections. Fig. 17 shows the computed stellar mass-density profiles at $t \approx 1$ Myr for similar calculations but including gas expulsion with parameters as

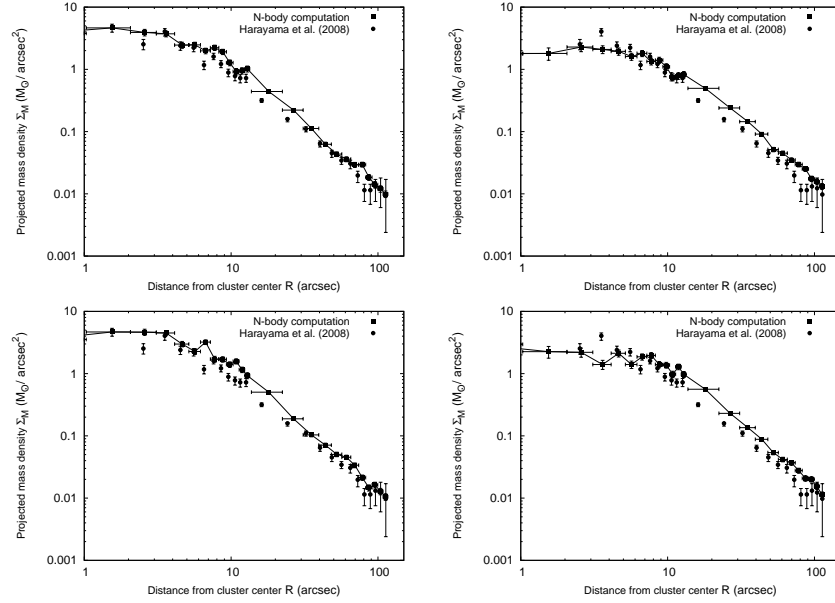


Fig. 17 Examples of surface mass-density profiles at $t \approx 1$ Myr for computed post-gas-expulsion configurations. Here, the systems evolve in a background residual gas potential (see Sec. 3) to form a star cluster with near-spherical core-halo structure (the CH-type morphology; see Table 3) within $t < 1$ Myr followed by residual gas dispersal at $\tau_d \approx 0.6$ Myr. The legends are the same as in Fig. 16. All these computed profiles agree well with the observed one for HD97950. These panels are reproduced from Banerjee & Kroupa (2015).

discussed in Sec. 2.2.1. As in Sec. 2.3.3, they agree reasonably with the observed profile of HD97950 (Harayama et al., 2008), particularly in the inner regions. Note that in Fig. 17, the “natural” matchings with the observed profile are obtained by *simply overlaying it with the computed profiles at 1 Myr without any scaling or fitting*, as in Banerjee & Kroupa (2014). The King-fit parameters to the observed and the computed profiles are also found to agree fairly.

We can now summarize the key inferences in the study discussed in this section, in logical sequence, as follows:

- A system of subclusters of total stellar mass $M_* \approx 10^4 M_\odot$ assemble into a (near) spherical core-halo star cluster by the age of HD97950 (*i.e.*, in $t < 1$ Myr) provided these subclusters are largely born over a region of scale length more compact than $R_0 \lesssim 2$ pc. This can happen, *e.g.*, in an intense starburst event at a dense “spot” in a molecular cloud.
- The initial sizes of the subclusters are constrained by the compact sections of molecular gas filaments or filament junctions which, in turn, determines the compactness of the final assembled cluster. Therefore, the mass density over the central region (within a virial radius) of the merged cluster is determined by the total stellar mass that is involved in its assembly.

- A “dry” merger of subclusters, *i.e.*, infall in absence of any residual molecular gas (all gas consumed into stars) always leads to a star cluster that is centrally overdense w.r.t. HD97950, even for the observed lower mass limit $M_* \approx 10^4 M_\odot$. This holds irrespective of the initial mode of subclustering.
- A substantial residual gas expulsion ($\approx 70\%$) after the formation of the merged system expands the latter to obtain a cluster profile that is consistent with the observed HD97950. With the lower stellar mass limit $M_* \approx 10^4 M_\odot$ and an SFE of $\varepsilon \approx 30\%$, the observed surface mass density profile of HD97950 can be fairly and optimally reproduced.

Notably, recent multi-wavelength observations of the Pismis 24 cluster of NGC 6357 (Massi et al., 2015) indicate that this cluster (age 1-3 Myr) contains distinct substructures which must have formed out of dense gas clumps packed within ≈ 1 pc radius. A similarly close-packed stellar substructures are found in the W3 complex (Román-Zúñiga et al., 2015). Jaehnig et al. (2015) also find that the stellar distribution in young clusters (1-3 Myr) tend to smoothen out with age and local stellar density. This indicates an appearance of these systems as closely packed stellar overdensities which disappear on a dynamical timescale as seen above.

In the context of any scenario that involves infall and merger of subclusters in their parent gas cloud, it is important to keep in mind that the *effective* SFE at the location of the merger (deepest part of the potential well, see above) can be much higher than 30%, depending on the stellar concentration in the newly merged cluster. This is true for the calculations presented in this section also. Note that this enhanced SFE is essentially a “population effect” and does not reflect that with which the star formation has actually taken place (*i.e.*, SFE within the gas clump(s)). The latter would be much smaller; $\lesssim 30\%$ (see Sec. 2.2.1).

NGC 3603 young cluster (HD97950) has formed essentially monolithically followed by a substantial and violent gas dispersal. The initial monolithic stellar distribution has either formed in situ or has been assembled “promptly” (in $\lesssim 1$ Myr) from closely packed (within $\lesssim 2$ pc) less massive stellar clusters (subclusters). Both scenarios are consistent with the formation of HD97950’s entire stellar population in a single starburst of very short ($\lesssim 10^5$ Myr) duration.

4 Globular clusters and the stellar IMF

The Milky Way (hereafter MW) contains approximately 160 globular clusters (hereafter GCs; see Harris 1996 for a compilation) most of which are nearly as old as the Universe. A major hot topic in astrophysics is to understand their birth and initial conditions. Here a discussion is provided which is consistent with and which is also based on the information gleaned from VYMCs as discussed in the previous sections.

Globular clusters appear to form a separate population of star clusters from those discussed above. However, Larsen (2002) has shown that star cluster formation extends from low stellar masses, $M_{cl} \lesssim 10^3 M_\odot$, to the most massive very young clusters observed in the nearby universe in interacting galaxies ($M_{cl} \gtrsim 10^5 M_\odot$) without a detectable change in their distribution with luminosity. It appears that star cluster formation is a continuous process in cluster mass, and that this mass distribution extends to high, GC-type masses in galaxies with high star formation rates (SFRs; Weidner et al. 2004; Randriamanakoto et al. 2013). However, three mass ranges are evident within each of which generically different physical processes play a role when clusters form (Kroupa & Boily, 2002): low mass clusters ($< \text{few } 10^2 M_\odot$ in stars) do not have O-stars (Weidner et al., 2013a) such that they are more likely to lose their residual gas adiabatically. Intermediate-mass clusters (few $10^2 M_\odot$ to $\approx 10^5 M_\odot$) contain one to many O-stars (Weidner et al., 2013a) which photoionize the residual gas and expel it probably explosively with a disruptive effect on the stellar component, while very massive clusters ($M > 10^5 M_\odot$) have, with increasing mass, an increasingly deep potential such that even photo-ionized plasma may not be able to leave the cluster within many initial crossing times (Baumgardt et al., 2008). These three regimes lead to different reactions of the clusters to the blow-out of the residual gas, such that an initially power-law mass function of embedded clusters evolves to a form with a turnover or flattening near $10^5 M_\odot$. Globular cluster-mass young clusters survive with a larger fraction of their stars and do not dissolve within a Hubble time (Elmegreen & Efremov, 1997; Kroupa & Boily, 2002; Baumgardt et al., 2008).

Such GC-precursors would have formed with very high densities, as the study by (Marks & Kroupa, 2010) suggests. This work is based on inferring the initial conditions of GCs subject to the constraint that their IMF for stars $\lesssim 1 M_\odot$ is canonical. Since GCs with a low concentration are observed to have a deficit of low-mass stars (De Marchi et al., 2007), and because neither a theoretical explanation through star formation is evident for this observation nor can it be explained with secular cluster evolution (fig.4 in Leigh et al. 2013), it is possible to infer that GCs may have formed mass segregated and increasingly compact with decreasing metallicity and that their initial radii are broadly consistent with Eqn. 9.

Consistency is also found independently by the first-ever N-body computation of two low-concentration GCs by Zonoozi et al. (2011, 2014). This work confirms that such GCs must have formed mass segregated and must have lost a substantial part of their low-mass stellar population during emergence from their embedded state. This leads to an understanding of the star-formation events within < 1 Gyr, as the first proto-Galactic gas cloud collapsed to form the MW population II halo and its associated present-day GCs at a time when the MW did not exist as the Galaxy (Marks & Kroupa, 2010).

But the results also imply that in order for the young GCs to emerge with a “damaged” (low-mass depleted) stellar mass function and low concentration, the IMF may have been increasingly top heavy with increasing density and decreasing metallicity (Marks et al., 2012). The remarkable result here is that these dependencies are well-consistent with the entirely independent results on the dependence of the IMF

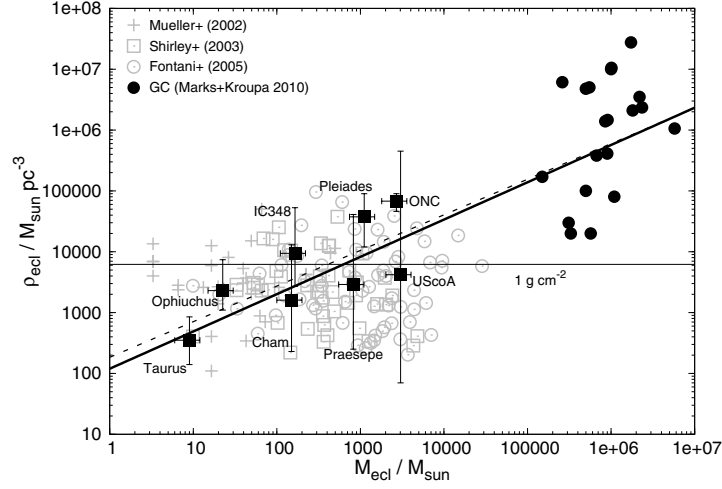


Fig. 18 Constraints on the initial volume-densities within the half-mass radius for the seven clusters (filled squares) versus the initial stellar mass as obtained by Marks & Kroupa (2012). The indicated errors in mass correspond to the observationally inferred present-day mass on the left end of a bar and two times the present-day mass on its right end, to be understood as an estimator of the possible range of initial mass. The filled circles are Galactic GCs. Underlaid as grey symbols are data of molecular cloud clumps as collated by Parmentier & Kroupa (2011). The clump masses are multiplied with a SFE of 1/3 to be comparable with the stellar masses and densities inferred in Marks & Kroupa (2012). The thin solid line is the threshold for massive star formation (Krumholz & McKee, 2008). The thick solid line is a least-squares fit to both the young cluster and GC values, implying that there exists a mass-radius relation for star cluster-forming cloud clumps. The dashed line shows the same when the GCs are excluded from the fit. This figure is reproduced from Marks & Kroupa (2012).

with density from the dynamical mass-to-light ratios and, independently, from the X-ray-source population of ultracompact dwarf galaxies (UCDs) by Dabringhausen et al. (2009, 2010, 2012). According to these results, the stellar IMF is canonical for SFR densities $\text{SFRD} < 0.1 M_{\odot}/(\text{pc}^3 \text{yr})$ and becomes increasingly top-heavy for stellar mass $\gtrsim 1 M_{\odot}$ with increasing density and decreasing metallicity (see eqn. 4.65 in Kroupa et al. 2013). These constraints on the variation of the stellar IMF with the physical conditions of star-forming cloud cores on scales of a parsec and time-scales of a Myr yield dependencies of M/L ratios of stellar populations which appear to be consistent with the observed values for the GCs of the Andromeda (Strader et al., 2011), as well as the high rate of type II supernovae in ULIRGs (Dabringhausen et al., 2012), as well as with the observed top-heavy galaxy-wide IMFs in star-forming galaxies within the IGIMF theory (Gunawardhana et al., 2011; Weidner et al., 2013b).⁸ Leigh et al. (2015) has demonstrated that the initial population of binary stars in very young GCs must have been very similar to the presently

⁸ From purely dynamical considerations, Banerjee & Kroupa (2012) also infer that VYMCs, in particular R136, should have born with the massive end of their IMF top-heavy. Continued dynamical interactions, resulting in mergers among the most massive stellar members in a massive

occurring binary population in the Milky Way, and the currently available result that the stellar IMF below a few M_{\odot} was also largely canonical (Marks et al., 2012), is consistent with this result and thus with the notion of an inherently largely universal process and outcome of star formation.

The generic formation of extremely massive, GC-like very young clusters is thus being understood increasingly better, but the detailed physical processes within these extremely dense (see Fig. 18) star-burst clusters remain a subject of intense study with major unsolved problems. In particular, the processes acting during the first few Myr in the highly dense plasma-star mixture, which may be pressurized from the ambient interstellar medium (ISM) in strongly star-bursting pre-galactic environments or in interacting galaxies, remains largely not understood (*e.g.*, Krause et al. 2013). The fact that increasingly massive GCs show evidence for increasingly complex metal abundance anti-correlations and spreads are rather certainly due to these extreme physical conditions (Georgiev et al. 2009; Charbonnel et al. 2014; also see Jiang et al. 2014 and references therein). But even the Hubble-time long dynamical evolution of GCs with a significant initial binary population may lead to hitherto not appreciated effects on the present-day chemical properties of GC stars (Jiang et al., 2014), while even intermediate-mass clusters and in particular very massive clusters may re-accrete ISM into their potential wells and this may occur repeatedly depending on the orbits of the clusters and of the ISM (Pflamm-Altenburg & Kroupa, 2009).

5 Concluding remarks: embedded vs. exposed young clusters

How VYMCs form is still an open question and even may not have a unique answer. As seen above, there are two primary directions of research that seek answer(s) to this question. The most physically detailed hydrodynamic calculations so far (including feedback; see Sec. 1), that led to star formation, currently range from a single proto-star to about $50M_{\odot}$ gas spheres, *i.e.*, less massive than the heaviest stellar member found in VYMCs (typically $> 100M_{\odot}$). Scaling the inferences all the way to the VYMC mass ($> 10^4M_{\odot}$) and size (\approx pc) is grossly unreliable since the physical behaviour of the feedback processes (radiation, magnetic field) are scarcely understood.

On the other hand, dynamical modelling of monolithic stellar systems, using direct N-body calculations can reach up to several 10^5M_{\odot} , with the current technology. As seen in the above sections, the main drawback in such studies is the simplified treatment of the residual gas (see Sec. 2.2). It is impressive, though, that such an approach remarkably reproduces the detailed observed properties of several young star clusters (see Sec. 2.3). This is also true if VYMCs (and young clusters in general) can be considered as formed via “prompt merging” of smaller subclusters in a background gas potential (see Sec. 3). In other words, a 1-3 Myr old VYMC can

cluster like R136 ($\approx 10^5M_{\odot}$), can make the stellar mass function top-heavy even at the present day (Banerjee et al., 2012b).

as well form from a highly subclustered stellar distribution, far from having spherical symmetry, provided the dynamical time (infall + violent relaxation; see Sec. 2.1) for the initial stellar system is sufficiently small. Note that the studies mentioned in Secs. 2.3 and 3 are currently the only theoretical studies in the massive cluster scale that provide direct and detailed agreements with observed clusters.

These results imply that once “blasted off”, the details of the gas hydrodynamics do not critically influence the dynamical evolution of the stellar system as long as cluster ages of the order of Myr are concerned. The key point is whether a rapid gas dispersal, with time-scale of the order of stellar crossing times (*c.f.* Table 1), should always occur in reality. The issue arises since compact embedded systems of several Myr age appear to be found throughout our Galaxy. An interesting example, in this respect, is the embedded W3 Main (hereafter W3M) cluster (Bik et al., 2014; Feigelson & Townsley, 2008). Located ≈ 2 kpc from the Sun, this is the most embedded region of the W3/W4/W5 star forming complex in the outer Galaxy, containing hyper-compact to extended HII regions. From the age estimates of the most massive (O-)star (IRS2), it can be inferred that W3M is forming stars since 2-3 Myr at least (Bik et al., 2014). It is argued that triggering as well as dynamical effects might keep the star formation ongoing in this system (Feigelson & Townsley, 2008). In particular, there are observational evidences that W3M is triggered externally by an expanding bubble from an OB association (Oey et al., 2005) and also internally by swept away material from OB stars (Wang et al., 2012). There are several similar-aged embedded clusters (*e.g.*, W33 complex, Messineo et al. 2015), but W3M is among the most well studied ones.

The existence of such systems appear to imply that not all forming stellar assemblies expel their residual gas promptly in an “explosive” (Kroupa, 2005) manner. For those cases this does happen, a VYMC like NGC 3603 is born, otherwise one is left with a “VYMC-aged” embedded system like W3M. For the latter case, the SFE would keep increasing with time as an increasing amount of gas is converted into and/or accreted onto proto-stars. It is currently unclear which physical processes (or absence of them) would delay the prompt gas expulsion. It could be the inherent properties of the natal gas (*e.g.*, its chemical abundances) and as well the surroundings that determines the fate of the star-forming clump. The presence or absence of ionizing O-stars could have been a plausible determining factor at a first glance, but several OB stars are found in W3M and other embedded clusters. The key question is as follows: *Despite the presence of ionizing OB stars in either case, why are some young star clusters (nearly) gas-free at an age of a few Myr and why are some others apparently deeply embedded in molecular gas at similar ages?*

For an explosive gas expulsion, the (compact) HII regions should rapidly engulf the densest (most populous) parts of the molecular clouds within their lifetimes; typically < 1 Myr (see Sec. 2.2.1; Banerjee & Kroupa 2013). Hence, the embedded proto-stellar population (or a significant part of it) should form in one episode (*i.e.*, with a small age spread) and within a compact enough region of the molecular cloud, typically < 1 pc (see Sec. 2.2.1; Banerjee & Kroupa 2013). The propagation of the (overlapped) HII region can be additionally powered by simultaneous presence of OB stars over a small region, further supporting compact and episodic star formation

for VYMCs. An interesting example in this regard is the RCW 38 cluster (DeRose et al., 2009; Kuhn et al., 2014), which is as compact as ≈ 0.1 pc (Eric Feigelson: private communication) and where only the central region is gas free, indicating that the residual gas might have just begun being expelled from the cluster. Indeed, as seen in Sec. 2.3, N-body computations that reproduce present-day VYMCs begin from such initial conditions. The stellar distribution in W3M, on the other hand, is more extended, > 1 pc, and contains several compact HII zones (Bik et al., 2014). This may also indicate that this region has formed a number of compact embedded clusters containing O/B-stars (see, *e.g.*, Testi et al. 1999). In future, more detailed observations will help to illuminate this possibility. Improved age estimates of the stellar population in W3M will be particularly important on this regard.

In other words, the fate of a newly hatched cluster might be governed by its scale length at birth. If the embedded stellar distribution is sufficiently compact (*e.g.*, if formed at a molecular gas filament junction; see Sec. 2.2.1), the natal gas can be blown apart when the UCHII region(s) engulfs (and hence ionizes) the scale length (Churchwell, 2002; Krumholz & Matzner, 2009; Banerjee & Kroupa, 2014). On the other hand, if the initial proto-stars are more widely distributed the gas may not be efficiently expelled and one is left with an embedded cluster. Of course, scale length may not be the only factor that determines if the gas expulsion “fails”. The gas expulsion can fail if the propagation of the HII region from around OB stars is stalled for any reason so that the embedding gas is ionized at most locally. Of course, if the newborn assembly is not massive enough so that no OB stars are formed, the gas would not be expelled even if the assembly is highly compact. This could be the case with several compact, low-mass embedded clusters (see, *e.g.*, Tapia et al. 2011). Note that a bimodal regime of cluster formation has been proposed earlier by Boily & Kroupa (2002) but in a somewhat different context.

If the fate of a newborn stellar assembly happens to depend on its length scale, a possibility as discussed above, the wider embedded systems can be expected to contain substructures. This is because, as seen in Sec. 3, the lifetime until which the substructures are erased to form a stellar cluster in dynamical equilibrium depends on the initial spatial span of the stellar distribution. This is consistent with the fact that substructures are found in many embedded clusters. If the embedded phase continues for a sufficiently long time the stellar system can virialize while remaining deeply embedded, as found recently (Foster et al., 2015). On the other hand, for a sufficiently extended system, the substructure can remain even if the gas is largely dispersed, *e.g.*, as seen in Cygnus OB2 (Wright et al., 2014).

Of course, it is important to re-consider the observationally inferred ages of the stellar members of the W3 Main and other embedded clusters *vis-à-vis* their distances, since age plays a crucial role in inferences such as above. This is true for gas-free VYMCs as well. For embedded clusters, the age estimates can be improved through even deeper and highly resolved observations, say, using *ALMA*. Such observations of dense molecular filaments and their junctions (or other sub-parsec scale dense structures) would reveal embedded clusters in them (or lack of them). For VYMCs, better parallax measurements with, *e.g.*, *Gaia* would provide independent distance measurements that would improve their age estimates. It is as

well important to better establish the depth of embedding of W3 Main and other embedded systems, in particular, whether the stellar system is actually embedded in gas or if it is a gas-free system inside or aside a molecular cloud, like, *e.g.*, the ONC and NGC 3603. Increased detection of HII regions and as well mapping the gas velocities over and surrounding embedded clusters would help to resolve this. For lightly-embedded and exposed star clusters as well as for embedded clusters, ongoing surveys such as the *MYSIX* (Massive Young Star-Forming Complex Study in Infrared and X-ray; Feigelson et al. 2013) would improve their age estimates, where X-ray observations provide additional constraints on the individual stellar ages (Getman et al., 2014). More detailed observations of both embedded and exposed clusters is the key to answer the fundamental question raised above, without which no concrete conclusions regarding the differences between embedded and exposed young clusters can be drawn.

The relation between exposed and embedded young clusters is currently unclear; the length scale over which the stellar population is hatched might play a role in determining whether the natal gas is expelled early (in < 1 Myr) or the stellar population remains embedded (slow gas dispersal and/or “gas consumption”). The detailed physical processes responsible for failing gas blow out in presence of the ionizing OB stars remain unclear. More detailed observations of embedded clusters like W3 Main is necessary to resolve this.

In summary, star formation is an intrinsically spatially and temporally correlated process which is evident to the astronomer as embedded clusters. The star formation process can be viewed as leading to a continuous distribution of embedded cluster masses where the most massive clusters, that can form, are constrained by the galaxy-wide SFR which, in turn, is controlled by the depth of the potential of the galaxy and thus the pressure in the turbulent interstellar medium (Elmegreen & Efremov, 1997; Klessen, 2001; Bonnell et al., 2011). VYMCs are a particularly shining part of this range of events, and GCs are the evolutionary fate of the most extreme VYMCs. The physics of the formation and of the emergence of VYMCs from their natal clouds carries through to the formation of GCs, but the extreme densities involved for them pose new and largely not-at-present-understood challenges. It is therefore, broadly speaking, not surprising that GCs show complex properties which are not evident in VYMCs. Finally, it is thanks to the continued decade-long algorithmic and mathematical progress achieved by Sverre Aarseth and Seppo Mikkola that the astrophysical community has now access to realistic N-body codes which allow us to address the issues discussed here. With the continuously improving and universally adaptable software platform like the “AMUSE” (Portegies Zwart et al., 2008), such N-body calculations can be made even more realistic (*e.g.*, introduce full hydrodynamical treatment) in foreseeable future.

References

- Aarseth, S.J. 2003, “Gravitational N-Body Simulations”. Cambridge University Press.
- Aarseth, S.J. 2012, *MNRAS*, 422, 841.
- Adams, F.C. and Fatuzzo, M. 1996, *ApJ*, 464, 256.
- Adams, F.C. 2000, *ApJ*, 542, 964.
- Alves, J. and Bouy, H. 2012, *A&A*, 547, A97.
- Amaro-Seoane, P., Konstantinidis, S., Freitag, M.D., et al. 2014, *ApJ*, 782, 97.
- Andersen, M., Zinnecker, H., Moneti, A., et al., 2009, *ApJ*, 707, 1347.
- André, P., Meñshchikov, A., Koenyves, V., et al. 2011, in Alfaro Navarro, E.J., Gallego Calvente, A.T., Zapatero Osorio, M.R. (Eds.) *Stellar Clusters & Associations: A RIA Workshop on Gaia*. Granada, Spain: IAA-CSIC, 321.
- André, P., Di Francesco, J., Ward-Thompson, D., et al. 2014, in Beuther, H., Klessen, R., Dullemond, C. and Henning, Th. (Eds.) *Protostars and Planets VI*, University of Arizona Press, Tucson, p.27.
- Banerjee, R. 2014, *A&A* submitted, arXiv:1409.7584 (preprint).
- Banerjee, S., Baumgardt, H. and Kroupa, P. 2010, *MNRAS*, 402, 371.
- Banerjee, S. and Kroupa, P. 2012, *A&A*, 547, A23.
- Banerjee, S., Kroupa, P. and Oh, S. 2012a, *ApJ*, 746, 15.
- Banerjee, S., Kroupa, P. and Oh, S. 2012b, *MNRAS*, 426, 1416.
- Banerjee, S. and Kroupa, P. 2013, *ApJ*, 764, 29.
- Banerjee, S. and Kroupa, P. 2014a, *ApJ*, 787, 158.
- Banerjee, S. and Kroupa, P. 2015, *MNRAS*, 447, 728.
- Bastian, N. and Silva-Villa, E. 2013, *MNRAS*, 431, L122.
- Bastian, N. and Strader, J. 2014, *MNRAS*, 443, 3594.
- Bate, M.R. and Bonnell, I.A. 2004, in Lamers, H.J.G.L.M., Smith, L.J., Nota A. (Eds.) *The Formation and Evolution of Massive Young Star Clusters*, (ASP Conf. Proc. 322). San Francisco: Astronomical Society of the Pacific, 289.
- Bate, M.R., 2009, *MNRAS*, 392, 590.
- Bate, M.R. 2012, *MNRAS*, 419, 3115.
- Bate, M.R., Tricco, T.S., Price, D.J. 2014, *MNRAS*, 437, 77.
- Baumgardt, H. and Kroupa, P., 2007, *MNRAS*, 380, 1589.
- Baumgardt, H., Kroupa, P. and Parmentier, G. 2008, *MNRAS*, 384, 1231.
- Bik, A., Stolte, A., Gennaro, M., et al. 2014, *A&A*, 561, A12.
- Boily, C. and Kroupa, P. 2002, in Grebel E.K., Brandner, W. (Eds.) *Modes of Star Formation and the Origin of Field Populations*, (ASP Conf. Proc. 285). San Francisco: Astronomical Society of the Pacific, 141.
- Boily, C. and Kroupa, P. 2003a, *MNRAS*, 338, 665.
- Boily, C. and Kroupa, P. 2003b, *MNRAS*, 338, 673.
- Bonnell, I.A., Smith, R.J., Clark, P.C. and Bate, M.R. 2011, *MNRAS*, 410, 2339.
- Brandner, W., 2008, in Beuther, H., et al., eds., “Massive star formation: Observations confront Theory”, ASP Conference Series, arXiv:0803.1974 (preprint).
- Charbonnel, C., Chantereau, W., Krause, M., et al. 2014, *A&A*, 569, LL6.
- Chini, R., Hoffmeister, V.H., Nasser, A., et al. 2012, *MNRAS*, 424, 1925.
- Churchwell, E., 2002, *ARA&A*, 40, 27.

- Crowther, P.A., Schnurr, O., Hirschi, R., et al. 2010, *MNRAS*, 408, 731.
- Dabringhausen, J., Kroupa, P. and Baumgardt, H. 2009, *MNRAS*, 394, 1529.
- Dabringhausen, J., Fellhauer, M. and Kroupa, P. 2010, *MNRAS*, 403, 1054.
- Dabringhausen, J., Kroupa, P., Pflamm-Altenburg, J. and Mieske, S. 2012, *ApJ*, 747, 72.
- Dale, J.E., Ercolano, B. and Bonnell, I.A. 2015, *MNRAS*, 451, 5506.
- De Marchi, G., Paresce, F., Pulone, L. 2007, *ApJ*, 656, L65.
- DeRose, K.L., Bourke, T.L., Gutermuth, R.A., et al. 2009, *AJ*, 138, 33.
- Dib, S., Kim, J. and Shadmehri, M. 2007, *MNRAS*, 381, 40.
- Duarte-Cabral, A., Dobbs, C.L., Peretto, N., et al. 2011, *A&A*, 528, A50.
- Elmegreen, B.G. and Efremov, Y.N. 1997, *ApJ*, 480, 235.
- Evans, C.J., Taylor, W.D., Hénault-Brunet, V., et al. 2011, *A&A*, 530, 108.
- Feigelson, E.D. and Townsley, L.K. 2008, *ApJ*, 673, 354.
- Feigelson, E.D., Townsley, L.K., Broos, P.S., et al. 2013, *ApJS*, 209, 26.
- Fellhauer, M. and Kroupa, P. 2005, *ApJ*, 630, 879.
- Foster, J.B., Cottaar, M., Covey, K.R., et al. 2015, *ApJ*, 799, 136.
- Fujii, M.S., Saitoh, T.R. and Portegies Zwart, S.F. 2012, *ApJ*, 753, 85.
- Fukui, Y., Ohama, A., Hanaoka, N., et al. 2014, *ApJ*, 780, 36.
- Fukui, Y., Torii, K., Ohama, A., et al. 2015, *ApJ*, arXiv:1504.05391 (preprint).
- Furukawa, N., Dawson, J.R., Ohama, A., et al. 2009, *ApJ*, 696, L11.
- Georgiev, I.Y., Hilker, M., Puzia, T.H., et al. 2009, *MNRAS*, 396, 1075.
- Getman, K.V., Feigelson, E.D. and Kuhn M.A. 2014, *ApJ*, 787, 109.
- Geyer, M.P. and Burkert, A. 2001, *MNRAS*, 323, 988.
- Girichidis, P., Federrath, C., Banerjee, R. and Klessen, R.S. 2011, *MNRAS*, 413, 2741.
- Girichidis, P., Federrath, C., Allison, R., et al. 2012, *MNRAS*, 420, 3264.
- Gunawardhana, M.L.P., Hopkins, A.M., Sharp, R.G., et al. 2011, *MNRAS*, 415, 1647.
- Harayama, Y., Eisenhauer, F. and Martins, F. 2008, *ApJ*, 675, 1319.
- Harris, W.E. 1996, *AJ*, 112, 1487.
- Haworth, T.J., Tasker, E.J., Fukui, Y., et al. 2015, *MNRAS*, 450, 10.
- Heggie, D.C. 1975, *MNRAS*, 173, 729.
- Heggie, D.C. and Hut, P. 2003, “The Gravitational Million-Body Problem: A Multidisciplinary Approach to Star Cluster Dynamics”. Cambridge University Press, Cambridge, UK.
- Hénault-Brunet, V., Evans, C.J., Sana, H., et al., 2012, *A&A*, 546, A73.
- Hennemann, M., Motte, F., Schneider, N., et al. 2012, *A&A*, 543, L3.
- Hill, T., Motte, F., Didelon, P., et al. 2011 *A&A*, 533, A94.
- Hillenbrand L. A. 1997, *AJ*, 113, 1733.
- Hillenbrand L. A. and Hartmann L. W. 1998, *ApJ*, 492, 540.
- Hills, J.G. 1975, *AJ*, 80, 809.
- Hills, J.G. 1980, *ApJ*, 235, 986.
- Hollyhead, K., Bastian, N., Adamo, A., et al. 2015, *MNRAS*, 449, 1106.
- Hurley, J.R., Pols, O.R. and Tout, C.A. 2000, *MNRAS*, 315, 543.
- Jaehnig, K.O., Da Rio, N. and Tan, J.C. 2015, *ApJ*, 798, 126.

- Jiang, D., Han, Z. and Li, L. 2014, *ApJ*, 789, 88.
- Jones B.F. and Walker M.F. 1988, *AJ*, 95, 1755.
- Klessen, R.S., Burkert, A. and Bate, M.R. 1998, *ApJ*, 501, L205.
- Klessen, R.S. 2001, *ApJ*, 556, 837.
- Krause, M., Charbonnel, C., Decressin, T., et al. 2013, *A&A*, 552, A121.
- Kroupa, P. 1995a, *MNRAS*, 277, 1491.
- Kroupa, P. 1995b, *MNRAS*, 277, 1507.
- Kroupa, P. 1998, *MNRAS*, 300, 200.
- Kroupa, P. 2001, *MNRAS*, 322, 231.
- Kroupa, P., Aarseth, S. and Hurley, J. 2001, *MNRAS*, 321, 699.
- Kroupa, P. and Boily, C.M. 2002, *MNRAS*, 336, 1188.
- Kroupa, P. 2005, in *The Three-Dimensional Universe with Gaia*, ed. C. Turon, K.S. O’Flaherty and M.A.C. Perryman (ESA SP-576; Noordwijk: ESA), 629.
- Kroupa, P., et al. 2013, in Oswalt, T.D. and Gilmore, G. (Eds.) *Galactic Structure and Stellar Populations* (Planets, Stars and Stellar Systems, Volume 5). Springer Science+Business Media Dordrecht (2013).
- Kruijssen, J.M.D. 2014, *Classical and Quantum Gravity*, 31, id.244006.
- Krumholz, M.R. and McKee, C.F. 2008, *Nature*, 451, 1082.
- Krumholz, M.R. and Matzner C.D., 2009, *ApJ*, 703, 1352.
- Krumholz, M.R., Bate, M.R., Arce, H.G., et al. 2014, in Beuther, H., Klessen, R., Dullemond, C. and Henning, Th. (Eds.) *Protostars and Planets VI*, University of Arizona Press, Tucson, p.243.
- Kuhn, M.A., Feigelson, E.D., Getman K.V., et al. 2014, *ApJ*, 787, 107.
- Küpper, A.H.W., Maschberger, T., Baumgardt, H. and Kroupa, P. 2011, *MNRAS*, 417, 2300.
- Lada, C.J., Margulis, M. and Dearborn, D. 1984, *ApJ*, 285, 141.
- Lada, C.J. and Lada, E.A. 2003, *ARA&A*, 41, 57.
- Larsen, S.S. 2002, *Extragalactic Star Clusters*, 207, 421.
- Leigh, N., Giersz, M., Webb, J.J., et al. 2013, *MNRAS*, 436, 3399.
- Leigh, N.W.C., Giersz, M., Marks, M., et al. 2015, *MNRAS*, 446, 226.
- Longmore, S.N., Kruijssen, J.M.D., Bastian, N., et al. 2014, in Beuther, H., Klessen, R., Dullemond, C. and Henning, Th. (Eds.) *Protostars and Planets VI*, University of Arizona Press, Tucson, p.291.
- Machida, M.N. and Matsumoto, T. 2012, *MNRAS*, 421, 588.
- Malinen, J., Juvela, M., Rawlings, M.G., et al. 2012, *A&A*, 544, A50.
- Marks, M. and Kroupa, P. 2010, *MNRAS*, 406, 2000.
- Marks, M. and Kroupa, P. 2012, *A&A*, 543, A8.
- Marks, M., Kroupa, P., Dabringhausen, J. and Pawlowski, M.S. 2012, *MNRAS*, 422, 2246.
- Marks, M., Leigh, N., Giersz, M., et al. 2014, *MNRAS*, 441, 3503.
- Massi, F., Giannetti, A., di Carlo, E. 2015, *A&A*, 573, id.A95.
- Messineo, M., Clark, J.S., Figer, D.F., et al. 2015, *ApJ*, 805, 110.
- Oey, M.S., Watson, A.M., Kern, K., et al. 2005, *AJ*, 129, 393.
- Oh, S. and Kroupa, P. 2012, *MNRAS*, 424, 65.
- Oh, S., Kroupa, P. and Banerjee, S. 2014, *MNRAS*, 437, 4000.

- Palla, F. and Stahler, S.W. 2002, *ApJ*, 581, 1194.
- Pang, X., Grebel, E.K., Allison, R., et al. 2013, *ApJ*, 764, 73.
- Parmentier, G. and Kroupa, P. 2011, *MNRAS*, 411, 1258.
- Patel, N.A., Curiel, S., Sridharan, T.K., et al. 2005, *Nature*, 437, 109.
- Pfalzner, S. 2009, *A&A*, 498, L37.
- Pfalzner, S. and Kaczmarek, T. 2013, *A&A*, 559, A38.
- Pflamm-Altenburg, J. and Kroupa, P. 2009, *MNRAS*, 397, 488.
- Portegies Zwart, S.F., McMillan, S.L.W., Nualláin, B. Ó., et al. 2008, *Lecture Notes in Computer Science*, 5102, 207.
- Portegies Zwart, S.F., McMillan, S.L.W. and Gieles, M. 2010, *ARA&A*, 48, 431.
- Price, D.J. and Bate, M.R. 2010, in *Plasmas in the laboratory and the Universe: Interactions, Patterns, and Turbulence*, (AIP Conf. Proc. 1242), 205.
- Raboud D. and Mermilliod J.-C. 1998, *A&A*, 329, 101.
- Randriamanakoto, Z., Escala, A., Väisänen, P., et al. 2013, *ApJ*, 775, L38.
- Rathborne, J.M., Longmore, S.N., Jackson, J.M., et al. 2014, *ApJ*, 795, L25.
- Rochau, B., Brandner, W., Stolte, A., Gennaro, M., et al. 2010, *ApJ*, 716, L90.
- Román-Zúñiga, C. G., Ybarra, J., Megias, G., et al. 2015, *ApJ*, arXiv:1507.00016 (preprint).
- Sana, H. and Evans, C.J. 2011, in Neiner, C., Wade, G., Meynet, G. and Peters, G. (Eds.) *Active OB Stars: Structure, Evolution, Mass Loss, and Critical Limits* (IAU Symp. 272). Cambridge Univ. Press, Cambridge, 474.
- Schneider, N., Csengeri, T., Bontemps, S., et al. 2010, *A&A*, 520, A49.
- Schneider, N., Csengeri, T., Hennemann, M., et al. 2012, *A&A*, 540, L11.
- Shin, J. and Kim, S.S. 2015, *MNRAS*, 447, 366.
- Smith, R., Goodwin, S., Fellhauer, M. and Assmann, P. 2013, *MNRAS*, 428, 1303.
- Spitzer, L.Jr. 1987, “Dynamical Evolution of Globular Clusters”, Princeton University Press.
- Stolte, A., Brandner, W., Brandl, B., et al. 2004, *AJ*, 128, 765.
- Strader, J., Caldwell, N. and Seth, A.C. 2011, *AJ*, 142, 8.
- Tafalla, M. and Hacar, A. 2015, *A&A*, 574, id.A104.
- Takahira, K., Tasker, E.J. and Habe, A. 2014, *ApJ*, 792, 63.
- Tapia, M., Roth, M., Bohigas, J., et al. 2011, *MNRAS*, 416, 2163.
- Tapia, M., Persi, P., Roth, M., et al. 2014, *MNRAS*, 437, 606.
- Testi, L., Palla, F. and Natta, A. 1999, *A&A*, 342, 515.
- Wang, Y., Beuther, H., Zhang, Q., et al. 2012, *ApJ*, 754, 87.
- Weidner, C. and Kroupa, P. 2004, *MNRAS*, 348, 187.
- Weidner, C., Kroupa, P. and Larsen, S.S. 2004, *MNRAS*, 350, 1503.
- Weidner, C., Kroupa, P. and Bonnell, I.A.D. 2010, *MNRAS*, 401, 275.
- Weidner, C., Kroupa, P. and Pflamm-Altenburg, J. 2013a, *MNRAS*, 434, 84.
- Weidner, C., Kroupa, P., Pflamm-Altenburg, J. and Vazdekis, A. 2013b, *MNRAS*, 436, 3309.
- Wright, N.J., Parker, R.J., Goodwin, S.P. and Drake, J.J. 2014, *MNRAS*, 438, 639.
- Wünsch, R., et al., 2011, *ApJ*, 740, 75.
- Zonoozi, A.H., Küpper, A.H.W., Baumgardt, H., et al. 2011, *MNRAS*, 411, 1989.
- Zonoozi, A.H., Haghi, H., Küpper, A.H.W., et al. 2014, *MNRAS*, 440, 3172.